GROWTH STUDIES OF VACUUM EVAPORATED THIN METAL FILMS DEPOSITED ON AMORPHOUS SUBSTRATES

Thesis for the Degree of Ph. D.

MICHIGAN STATE UNIVERSITY

JAMES A. BAUMBACH

1967

THESIS

This is to certify that the

thesis entitled

Growth Studies of Vacuum Evaporated Thin
Metal Films Deposited on Amorphous Substrates

presented by

James A. Baumbach

has been accepted towards fulfillment
of the requirements for

Ph.D. **degree in** Chemistry

Carl H. Brubaker, Jr.
Major professor

Date February 23, 1968

O-169

GROWTH STUDIES OF VACUUM EVAPORATED THIN METAL FILMS DEPOSITED ON AMORPHOUS SUBSTRATES

By

James A. Baumbach

A THESIS

Submitted to
Michigan State University
in partial fulfillment of the requirements
for the degree of

DOCTOR OF PHILOSOPHY

Department of Chemistry

1967

G 47203
5-20-68

TABLE OF CONTENTS

Page

LIST OF FIGURES iii

LIST OF TABLES v

ACKNOWLEDGMENTS vi

ABSTRACT viii

I. INTRODUCTION 1

A. Objectives 1

B. Background 1

C. Theory 6

1. Embryo formation 6
2. Adatom concentration 7
3. Critical nucleus 9
4. Nucleation rate 11
5. Statistical contributions 15

II. EXPERIMENTAL 18

A. Background 18

1. Substrates 18

a. Steps and surface defects 18
b. Ionic character 19
c. Substrate cleanliness 21
d. Substrate interaction 22
e. Adsorbed gases on substrates . . 27

2. Vacuum evaporator 27

B. Methods 29

1. Vacuum chamber 29
2. Evaporation assembly 31
3. Thickness monitor reproducibility . . 37

C. Procedure 40

1. Filament temperature 40
2. Substrate preparation 42
3. Film deposition parameter measurements 45
4. Electron microscope sample preparation 45

III. INTERPRETATION OF OBSERVATIONS 47

A. Indium and lead films 47

B. Tin films 62

C. Indium-lead films 65

D. Contact angles 69

IV. ANALYSIS AND RESULTS 72

A. Analysis 72

B. Results 74

V. CONCLUSIONS 92

VI. PROPOSED WORK 95

VII. LIST OF REFERENCES 98

LIST OF FIGURES

Figure		Page
1.	Lead in indium diffusion curves	24
2.	Replicas of indium surfaces prior to lead evaporation	26
3.	Evaporation chamber	30
4.	Evaporation source	33
5.	Substrate holder and evaporation mask for electrical resistance measurements . . .	34
6.	Substrate insertion mechanism and shutter	36
7.	Film resistance dependence on film thickness for indium deposited films . .	38
8.	Replicas of indium films for resistance measurements	39
9.	Deposition rate dependence upon filament temperature	43
10.	Growth of indium films	48
10.	Continued	49
11.	Growth of lead films	50
11.	Continued	51
12.	Fresh nucleation on re-exposed substrate following coalescence, and hexagonal indium crystallite	54
13.	"Milky" indium film	58
14.	100 cps of indium evaporated by the electron microscope beam	59
15.	750 cps indium film evaporated by the electron microscope beam	60

16. Growth of tin film 63

16. Continued 64

17. Indium film grown on 100 cps lead 66

17. Continued 67

18. Electron diffraction patterns 68

19. Three-dimensional electron micrographs of metal films on silicon monoxide substrates 70

20. Indium film No. 1. Indium deposited upon SiO prepared *in situ* 75

20. Continued 76

21. Indium film No. 2. Indium deposited upon SiO prepared *in situ* 78

21. Continued 79

22. Indium film No. 3. Indium deposited on SiO prepared in a separate chamber 81

23. Indium film No. 4. Indium deposited on SiO prepared in a separate chamber 83

24. Lead film grown upon SiO prepared in a separate chamber 85

25. Tin film grown upon SiO prepared *in situ* . . 87

25. Continued 88

26. Indium deposited upon 100 cps of lead 90

26. Continued 91

LIST OF TABLES

Table Page

1. Monitor Thickness-Electrical Resistance Data 41

2. Film Thickness, Deposition Rate and Resistivity Data 41

3. Occurrence of Predominant Peaks for Indium Film No. 1 74

4. Occurrence of Predominant Peaks for Indium Film No. 2 77

5. Occurrence of Predominant Peaks for Indium Film No. 3 80

6. Occurrence of Predominant Peaks for Indium Film No. 4 82

7. Occurrence of Predominant Peaks for Lead Film 84

8. Occurrence of Predominant Peaks for Tin Film 86

9. Occurrence of Predominant Peaks for Indium Film on Lead 89

ACKNOWLEDGMENTS

I wish to express my sincerest gratitude to my thesis advisor, Professor C. H. Brubaker, for his patience and understanding which have contributed so much toward the completion of this study. I especially acknowledge Dr. C. T. Wei for the many stimulating and challenging discussions that helped to clarify my thoughts and to guide my expression of them. For his instructions on the electron microscope and his generous supply of microscope filaments, I would like to thank Dr. D. E. Scherpereel.

My deepest appreciation is extended to the Office of Engineering Research for the use of their machine shop, office space, and vacuum evaporation equipment. To the staffs of the machine shops in Engineering Research and in the Department of Physics, special thanks is given for the numerous pieces of equipment built for this study. I would also like to express my fond memories of Mr. Frank Betts whose instruction in equipment building was most appreciated. Acknowledgment also goes to Mrs. V. Kitzman for her help in the data analysis, and to the Waukesha Foundry Company, Waukesha, Wisconsin, for the materials supplied.

To my wife, for whom no words could describe the special place she occupies in my research and in my life, I am most deeply indebted.

The financial support of the National Science Foundation and Dr. S. K. Haynes is greatfully acknowledged.

ABSTRACT

GROWTH STUDIES OF VACUUM EVAPORATED
THIN METAL FILMS DEPOSITED ON
AMORPHOUS SUBSTRATES

by James A. Baumbach

The growth characteristics for metal films of indium, lead and tin, and a bimetallic film of lead and indium have been investigated for a range of film thicknesses. The films were prepared on amorphous substrates by thermal evaporation at residual pressures of 2×10^{-6} torr and lower. They were found to exhibit similar characteristics, with the minor exception that tin becomes continuous much sooner than the other metals for a comparable quantity of deposited metal. During the archipelago stage the characteristics of growth are defined by three secondary stages. The first stage of growth occurs just after nucleation when the film contains uniform, non-interacting nuclei. The nuclei continue to grow primarily by the addition of migrating surface atoms. The second stage begins when intermediate sized nuclei coalesce to form larger ones. Finally, coalescence of large islands and large island assimilation of small nuclei mark the third growth stage. In addition, a method for contact angle measurement within the electron microscope, and the discovery of non-assimilated nuclei beneath large islands are discussed.

I. INTRODUCTION

A. Objectives

The objectives of this research were to produce indium and other metal films by thermal evaporation upon amorphous substrates, and to study in detail the nucleation and growth processes involved.

Since both nucleation and growth are being studied together, a desirable experiment should include aspects of each, and at the same time, yield quantitative results for comparison with present nucleation theory. To meet these requirements, the stage of growth chosen for examination starts with nucleation and ends before the film becomes continuous. Each film therefore, was prepared with varying thicknesses, while other parameters, e.g. substrate temperature, pressure and deposition rate, were held constant. The tabulated results include the quantity and size of each cluster grouping, the amount of coverage of the substrate for each cluster size, and an estimate of the contact angle. Finally, the type of cluster interaction observed is discussed along with a description of a possible mechanism for the interaction.

B. Background

Heterogeneous nucleation was discovered by R. W. Wood (1) while studying the electrical discharge

phenomena of metal vapor. When a portion of the glass vacuum apparatus was cooled to prevent the walls from collapsing, metal was found to deposit in this area. From his studies with cadmium, Wood found that once a layer of metal formed at reduced temperatures, subsequent impinging cadmium atoms continued to condense even at room temperature. That is, cadmium would not nucleate on a glass surface when the surface temperature exceeded a critical value. To account for the inhibited film growth, Wood postulated a mechanism based on atom reflection from the substrate. In other words, the metal vapor atom strikes the surface and rebounds through an elastic collision.

Langmuir (2) confirmed the existence of a critical temperature for metal film nucleation and was able to relate the temperature to the evaporation rate. Because the critical temperature was found to increase with increasing evaporation rate, Langmuir concluded that the primary mechanism which inhibited film nucleation and growth was one of adsorption and re-evaporation of the metal atom rather than atom reflection.

The effects of substrate temperature and condensation rate upon film density are discussed by Thun (3). Over a range of temperatures and deposition rates, many metals exhibit either a maximum or minimum in density and electrical conductivity. As the substrate temperature increases, the deposited film contains fewer

lattice faults as a result of increasing crystallite size. It is assumed (3) that the greatest concentration of structural faults is located at the grain boundaries. Therefore, film density decreases with an increasing number of grain boundaries, and densities as low as 82% of the bulk material may be obtained as a result of low temperature deposition in the presence of residual gases. For many metals, a maximum in film density and a corresponding minimum in film resistivity occur at substrate temperatures between 150°C and 300°C. The density decrease at still higher temperatures cannot be explained entirely on the basis of an increasing number of lattice faults. For this reason it appears that preferential growth of certain lattice planes within the grain and increased oxidation contribute significantly to the density decrease.

Edgecumbe (4) has reviewed density values for thermally evaporated Cu, Ag, Au, In and Ni-Fe films and has reported that they range as low as 30% below bulk values. He suggested that a possible source of error in the density values may arise from the use of indirect methods of thickness measurements.

Variations in the rate of deposition produce similar fluctuations in the density and resistivity. When the rate is low, surface atoms have more time to reach clusters of lower free energy, thereby producing a rough and loosely packed film. With increasing rates,

the density increases and the film becomes smoother. Finally, at higher kinetic energies, the impinging metal atoms are buried at random sites in the substrate by successively arriving atoms. Because a large activation energy is necessary to reorder the buried atoms, the resulting film has a considerable number of lattice faults.

During the growth of metal films, small clusters on the substrate joined together as if they were liquid metal droplets. The liquid-like behavior of the clusters has been investigated by Pashley and Stowell (5) with cinematography. During the growth of silver layers prepared inside the electron microscope, the clusters were observed to behave as if they were composed of liquid drops; that is, nuclei of about 100Å across continued to grow in size until they touched and coalesced. The resulting island was larger, but it maintained the outline of the two or more smaller islands. Diffraction contrast studies of this phenomenon indicated that changes in the structure of the islands were taking place but that the islands did not become liquid, even momentarily, as they coalesced. Also, it was noted that relatively little fresh nucleation occurred during the observation.

As the islands continue to coalesce and the coverage of the substrate increases, a point is reached when fresh nucleation ceases even though a relatively large

amount of substrate is still exposed. These exposed areas, in the form of long canals, are uniform in width and close suddenly as more atoms are added to the film (6). According to McLauchlan, et al. (7), the four stages of film growth are nucleation, archipelago, labyrinth and closing.

Most nucleation theory predicts that the nucleation rate is proportional to the number of sites available on the substrate (8). From the preceeding experimental results, it is obvious that not all exposed substrate area is available for nucleation. For any given system, therefore, the nucleation rate must eventually go to zero as a result of the time dependence of the availability of sites. Robins and Rhodin (9) have formulated the rate at which nucleation sites become occupied:

$$dN/dt = [(N_o - N)/N_o]\, I, \qquad 1$$

where N is the number occupied at time t, N_o is the maximum number available and I is the rate at which atoms arrive at these sites. Since I is time independent, the solution is

$$N = N_o[1 - \exp(-tI/N_o)]. \qquad 2$$

During film formation on an amorphous substrate, coalescence re-exposes substrate areas whenever the surface tension of the metal approaches or exceeds the interfacial energy between the crystal and the substrate. At the beginning of the evaporation, the initial

buildup of particles is due to unrestricted nucleation at all sites. Following the buildup, coalescence begins and the number of particles on the substrate decays until a sufficient amount of substrate is again exposed. The amount is dependent upon the diffusion distance of adsorbed atoms and the chance of their colliding with a critical nucleus before reaching a more stable island. This process is repeated until the labyrinth stage, at which time the film islands remain more or less stationary and nucleation ceases.

C. Theory

1. Embryo formation

Nucleation theory in general is concerned with the net process of forming a crystallite embryo of i atoms from either single atoms or molecules. The reaction which takes place on a substrate during metal film formation is

$$iA = A_i, \quad (3)$$

where A is the adsorbed monomer and A_i is the embryo of i atoms. The above reaction re-written in terms of the number of clusters of i atoms per square centimeter, n_i, that may form from a number of adsorbed monomers (adatoms) per square centimeter, n_1, is

$$in_1 = n_i. \quad (4)$$

Taking into account all clusters which may appear during the initial formation process,

$$i(n_1 + \Sigma n_i)n_1 = (n_1 + \Sigma n_i)n_i, \quad (5)$$

where the term $(n_1 + \Sigma\, n_i)$ accounts for all species present on the substrate.

Rearranging 5,

$$i[n_1/(n_1 + \Sigma\, n_i)] = n_i/(n_1 + \Sigma\, n_i) \qquad 6$$

from which the equilibrium constant is obtained (10),

$$K = [n_i/(n_1 + \Sigma\, n_i)]/[n_1/(n_1 + \Sigma\, n_i)]^i. \qquad 7$$

Since the number of adatoms, n_1, present at any time is greater than all other crystallite sizes, the equilibrium constant reduces to n_i/n_1.

Employing the van't Hoff reaction isotherm

$$\Delta G = -kT \ln K, \qquad 8$$

$$\Delta G = -kT \ln(n_i/n_1), \text{ and finally} \qquad 9$$

$$n_i = n_1 \exp(-\Delta G/kT). \qquad 10$$

2. Adatom concentration

The time dependence of the single adatom concentration on the substrate may be described by the difference between the impingent and desorption fluxes

$$dn_1/dt = J_i - J_{des}. \qquad 11$$

The impingent flux, J_i, is a function of filament temperature and is time independent, while the desorption flux, J_{des}, is defined as the ratio of the adatom concentration to the mean stay time of an atom on the substrate (11)

$$J_{des} = n_1/\tau_s. \qquad 12$$

Substituting in equation 11 for the desorption flux

$$dn_1/dt = J_i - n_1/\tau_s, \qquad 13$$

where the mean stay time may be approximated by

$$\tau_s = \nu^{-1}\exp(\Delta G_{des}/kT). \qquad 14$$

In equation 14, ν is the vibrational frequency of the adatoms, T is the substrate temperature, and ΔG_{des} is the free energy of activation of desorption. The solution (8) to equation 13, as a function of the exposure time, t, is

$$n_1 = J\tau_s[1 - \exp(t/\tau_s)]. \qquad 15$$

In the usual experiment*, $t \gg \tau_s$, and as a result, n_1 is equal to $J\tau_s$. Therefore, n_1 represents the metastable concentration of adatoms which remains constant until stable nuclei begin to form. While the concentration is constant, the re-evaporation flux is equal to the impingent flux (11, 12),

$$J = p/(2\pi mkT)^{1/2} = n_1/\tau_s = n_1\nu\,\exp(-\Delta G_{des}/kT), \qquad 16$$

where p is the equivalent vapor pressure at the surface temperature T, m is the atomic mass of the metal and k is Boltzmann's constant.

From equation 16, p and n may be related to their respective thermodynamic equilibrium values for the bulk condensate by assuming the monomer is the predominant species in both the vapor (13) and the adsorbed states.

$$p/p_e = n_1/n_{1e} = S, \qquad 17$$

where S is the supersaturation ratio.

---

*For other experimental conditions see reference (8).

3. Critical nucleus

The thermodynamic properties of embryo and critical nuclei are treated macroscopically in order to estimate their free energies. However, it is carefully pointed out that such an estimate is applied to very small clusters, sometimes containing as few as twenty-four atoms, and therefore, constitutes only a gross approximation. For a group of twenty-four atoms, the nearest neighbors surrounding a central atom are in equilibrium with the vapor. To avoid this problem, Gibbs limited his calculations to large clusters and indicated the cluster-vapor boundary in such a way that the undefined atomic region between the crystal and vapor was negligible compared to the crystal radius.

Since the necessary potential energy and internal partition functions (14) for small clusters must yet be determined, the Gibbs-Volmer model is applied in this case.

The free energy of formation of spherical cap-shaped embryos containing i atoms* according to the Gibbs (15)-Volmer (16) model is

$$\Delta G = \pi r^2 \sin\theta(\sigma_{c-x} - \sigma_{x-v}) + 4\pi r^2 \phi_1(\theta)\sigma_{c-v} + (4\pi/3) r^3 \phi_2(\theta)\Delta G_v + \Delta G_s, \qquad 18$$

where r is the radius of the sphere, θ is the contact angle, σ is the interfacial energy between the crystal and the substrate, c - x between the substrate

*The number of atoms in an embryo of radius r is $4\pi r^3/3\Omega$.

and vapor, x-v, and between the crystal and vapor, c-v; G_v is the Gibbs free energy difference per unit volume of liquid between the supersaturated vapor of pressure, p, and the bulk liquid equilibrium vapor pressure, p_e.

$$\Delta G_v = -(kT/\Omega)\ln(p/p_e), \qquad 19$$

where Ω is the molecular volume. A combination of equations 17 and 19 results in

$$\Delta G_v = -(kT/\Omega)\ln(S). \qquad 20$$

Considering equation 18 as a sum of free energy terms, we obtain

$$\Delta G = \Delta G_1 + \Delta G_2 + \Delta G_3. \qquad 21$$

The first term describes the surface free energy relationship between the three phases.

$$\Delta G_1 = \pi r^2 \sin\theta(\sigma_{c-x} - \sigma_{x-v}) + 4\pi r^2 \phi_1(\theta)\sigma_{c-v}, \qquad 22$$

where the geometric function, ϕ_1, is equal to $(1 - \cos\theta)/2$. According to Gibbs, the interfacial energies are related to the contact angle by

$$\sigma_{x-v} = \sigma_{c-x} + \sigma_{c-v}\cos\theta. \qquad 23$$

The second energy term concerns the negative of the volume free energy

$$\Delta G_2 = (4\pi/3)r^3\phi_2(\theta)\Delta G_v, \qquad 24$$

where ϕ_2 is given by

$$\phi_2 = [2 - 3\cos\theta + \cos^3\theta]/4. \qquad 25$$

The contact angle and ϕ_2 represent the "catalytic potency" (17) of the substrate, that is, an angle of 0° corresponds to complete "wetting" of the substrate and nucleation will be very rapid (10). On the other hand,

if the angle equals 180° there is essentially no "wetting" of the substrate and the nucleation is homogeneous. The third energy term, ΔG_3, is a statistical contribution and will be discussed later.

The free energy of spherical cap formation passes through a maximum as the radius of the cap is increased atom by atom. Therefore, maximizing the free energy of formation, equation 18, with respect to r and neglecting the statistical contribution, one obtains the radius, r*, for the critical nucleus

$$r^* = -2\sigma_{c-v}/\Delta G_v. \qquad 26$$

The free energy of the critical nucleus is then given by

$$\Delta G^* = 16\pi\sigma_{c-v}^3/3\Delta G_v\phi_2. \qquad 27$$

In accordance with equation 10, the concentration of critical nuclei n_i^* present in terms of the adatom concentration is

$$n_i^* = n_1 \exp(-\Delta G^*/kT). \qquad 28$$

4. Nucleation rate

The rate at which stable growing nuclei are formed, I*, is given by the product of the diffusion rate, ω*, of single atoms to a critical size nucleus, the concentration of critical nuclei, n_i^*, and a non-equilibrium factor, Z.

$$I^* = Z\omega^* n_i^*. \qquad 29$$

The rate expression is based upon a steady state kinetic problem which takes into account the details of raising an embryo from one crystallite size to another. The

steady state may be described mathematically by reducing the supercritical cluster atom to the monomer. The non-equilibrium factor,

$$Z = (\Delta G^*/3\pi kTi^{*2})^{1/2}, \qquad 30$$

is related to the ratio of steady state to metastable equilibrium concentration of critical nuclei and the gradient of nuclei. The factor has been shown by Hirth (18) to be essentially unity for the nucleation of metal vapors upon substrates.

The process of adding single atoms to the critical nucleus may occur by direct addition from the vapor and/or by surface diffusion of an adatom. The nucleation rate by surface diffusion has been shown (20) to be greater than by direct addition from the vapor by a factor, f, where

$$f = \exp[(\Delta G_{des}^* - \Delta G_{sd}^*)/kT]. \qquad 31$$

Since the surface migration process is dominant, the diffusion rate is given by

$$\omega^* = (n_1 2\pi r^* a \sin\theta)\nu \exp(-\Delta G_{sd}^*/kT), \qquad 32$$

where G_{sd}^* is the free energy of activation of surface diffusion in a localized model for atoms, the factor in parenthesis accounts for the number of adatoms adjacent to the critical nucleus, and the rest is the jump frequency of the adatom to join the nucleus, where each jump is equal in length to one atomic diameter, a, (21). Solving for n_1 in equation 16 and substituting the

result in equation 28,

$$n_i^* = \nu^{-1}p/(2\pi mkT)^{1/2}\exp(\Delta G_{des}^* - \Delta G^*)/kT. \qquad 33$$

Substituting for ω^* and n_i^* in 29,

$$I^* = Cp\ \exp[(\Delta G_{des}^* - \Delta G_{sd}^* - \Delta G^*)/kT], \qquad 34$$

where $$C = Z(n_o 2\pi r^* a\ \sin\theta)(2\pi mkT)^{-1/2}. \qquad 35$$

For a given system, C is essentially constant for a range of pressure and temperature and assumes a value of about 10^{17} $dyne^{-1}sec^{-1}$(21).

Rhodin and Walton (22) have criticized the nucleation theory set forth by Pound, Simnad and Yang (20), as presented in part in this paper's theory discussion, for the following reasons: First, there is little difference between their approach to the nucleation rate calculation and the classical treatment set forth by Volmer and Weber (23) and Becker and Doering (19). Second, Pound, et al., (20) assumed that the shape of the nucleus did not change and that bulk thermodynamic properties could be used to compute the free energy of nucleus formation. Third, in using the theory, it was found (24) that the nucleation rate is difficult to perceive for a small nucleus which, calculated from the theory, contains only nine atoms. In general, Rhodin and Walton (22) consider such a theory "non applicable" to the nucleation of metal vapors upon an inert substrate.

In its stead, Walton (25) has obtained an expression for the nucleation rate

$$I = R\ a^2 n_o (R/\nu n_o)^{i^*}\exp[(i^* + 1)\Delta G_{ad} + \Delta G_i^* - \Delta G_{sd}/kT] \qquad 36$$

where R is the incident rate in the form of monolayers per second, n_o is the density of adsorption sites, i^* is the number of atoms in the critical nucleus, ΔG_{ad} is the heat of adsorption, ΔG_{i^*} is the energy of dissociation of the critical nucleus, and other symbols have their usual meaning. Accordingly, the rate expression (rewritten in the terminology of this paper) avoids the objectionable assumptions given above. Moreover, unlike the Volmer and Weber-Becker and Doering theory, the Walton treatment does not yield an analytic expression for ΔG_{i^*} nor i^*. Therefore, one must write down expressions for the rate for different sized clusters on a trial and error basis. At the limit of high supersaturations, the critical nucleus should be a single atom, and therefore, when a pair of atoms form they will, on the average, continue to grow. When the supersaturation is decreased, e.g. increasing the substrate temperature or decreasing the incident rate, the probability of continued growth is lowered such that the two atom clusters will have an equally likely chance of decaying. Below this supersaturation, the pair of atoms now represents the critical nucleus. One then continues this process until he reaches the desired nucleus size.

Gretz and Pound (8) investigated the shape of small nuclei at a resolution of about 20Å using a tungsten substrate-emitter tip in a field emission microscope.

They concluded that the critical nucleus should indeed be represented by a spherical cap; however, because of the difference in contact angles between the small cluster on the tungsten substrate and the bulk metal on tungsten, a line tension effect was postulated. The line tension term, which was derived from the minimization of the Helmholtz energy of an embryo with respect to variations in the contact angle at constant volume, appeared in the interfacial energy, contact angle formula

$$\sigma_{s-v} = \sigma_{c-s} + \sigma_{c-v}\cos\theta + \sigma_t/r \sin\theta, \qquad 37$$

where σ_t was the line tension term. It was found that coherency constraints affect the nucleation on substrates very little.

5. Statistical contributions

So far, nucleation theory has been used to describe embryo formation and distribution among available energy levels corresponding to the adatom concentration. Second, it has also been used to determine the size of the critical nucleus and the size relation to the supersaturation ratio. Third, the rate at which the critical nucleus forms is found to be proportional to the available nucleation sites. It is the last point which will be considered in this section.

Lothe and Pound (26) have treated the statistical contribution to nucleation theory in the following manner. In the crystallite nucleation on solid substrates

from the vapor, the standard state of the embryo is taken as the pure metal and the number is equal to the concentration of adsorbed monomers, n_1. The number of ways, W, of distributing n monomers among n_o sites on the solid substrate is

$$W = n_o!/n_1!(n_o - n_1)!. \qquad 38$$

The contribution to the free energy of formation is

$$\Delta G_d = -(kT/n_1)\{n_o \ln[(n_o-n_1)/n_o] + n_1 \ln[n_1/(n_o-n_1)]\}. \qquad 39$$

In the usual experiment $n_o >> n_1$ and

$$\Delta G_d = -kT\ln(n_o/n_1), \qquad 40$$

where n_o/n_1 represents the factor in the increase in equilibrium concentration of nuclei. Also, since $n_1 >> n_i$, n_1 disappears from the equilibrium concentration expression

$$n_i^* = n_o \exp(-\Delta G^{*\prime}/kT). \qquad 41$$

However, according to Robins and Rhodin (9), the number of available nucleation sites on a crystalline substrate are finite and limited, and the number of sites and the rate at which they become occupied is given by equations 2 and 1 respectively. During the time when all available substrate nucleation sites are effectively covered by growing stable clusters, little or no fresh nucleation occurs. However, when coalescence takes place, large areas of the substrate are left exposed and nucleation resumes until these areas are also covered. Initial nucleation is rapid and should follow the kinetics as outlined by Robins and Rhodin (9).

Then, as the clusters reach a certain size, the value of which depends upon the contact angle, surface tension of the metal, and the distance the migrating surface atom travels before coming in contact with a stable cluster, the re-exposed substrate will again permit nucleation with Robins and Rhodin kinetics.

II. EXPERIMENTAL

A. Background

1. Substrates

The substrate upon which a metal is deposited during vacuum evaporation is of primary importance to the growth and structure of thin metal films. The substrate may influence film properties in a number of ways, namely (a) the steps and surface defects on cleaved ionic substrates (rocksalt, etc.) provide areas of increased nucleation sites; (b) the ionic character of the substrate may interact with valence electrons to inhibit or promote nucleation; (c) substrate cleanliness determines the extent to which metal films bond with the substrate; (d) reactions and bond-forming character of the substrate during prenucleation permit thinner and more continuous films to be prepared; (e) adsorbed layers of gases impair surface mobility of metal atoms.

a. Steps and surface defects

Metal nuclei are formed along steps of cleaved ionic salts and "decorate" such steps with concentrations of nuclei far greater than in areas which are essentially flat. In this manner, monatomic steps have

been detected through decoration with gold nuclei (27, 28, 29). Although the initial concentration of nuclei is greatest along these steps, the number of crystallites decreases in subsequent stages through coalescence, and preferred growth at the steps is no longer detectable. The first nuclei to appear are quite uniform in size and remain so during continued growth. At the same time, there is very little fresh nucleation in spite of the increasing distance between crystallites, which suggests that the nature of the substrate changes after it has been covered and re-exposed to an impingent atomic beam. Because of three-dimensional growth during coalescence, the newly formed island occupies less substrate than the sum of the parent islands before coalescence.

b. Ionic character

The type and quantity of ionic charge present on the substrate may offer a clue to the change in the nature of the re-exposed substrate cited above. Hill (30) investigated the effect on thin gold films of an electrical charge induced on glass substrates at the time of evaporation. During the experiment the electrical charge disappeared as gold condensed. When the charge was no longer detected, the substrate was exposed a few seconds longer to establish nuclei location, and then the experiment was terminated. Since both ends of the glass surface facing the evaporation source were

polarized, areas appeared on the surface with equal but opposite charges. It was found that the positively charged portion of the surface contained a density of nuclei nearly equal to the density of the charge, whereas the negatively charged surface contained one-third the number of nuclei as charges. Because of the grouping of nuclei around glass imperfections, a second count of the negatively charged areas was taken which neglected the grouped nuclei, and a new ratio of 30:1 was found.

The charge present in the vapor beam represents only 10^{-8} of the total impingent flux and is discounted as a possible mechanism for nucleation on electrically charged surfaces. The results are consistent with nucleation at surface dipoles, where the valence electron from a vapor atom is held by a positive site, thereby providing a significant number of nucleation sites. Nucleation on ionic substrates may be influenced by the residual charge on the freshly cleaved surface; however, highly oriented films form only when heated above a critical temperature (31, 32). Since the electrical charge on a substrate may be dispelled by baking, charge alone is not the most significant feature of the ionic substrate in oriented film deposits. Other aspects of oriented films and substrate bonding are considered by van der Merwe (33).

c. Substrate cleanliness

A definition of an atomically clean surface is given by Allen *et al.* (34). A clean surface is essentially free of contamination, except for a small percentage of a monolayer of foreign atoms, which are either adsorbed on the substrate or substitutionally replace surface atoms in the parent lattice. This definition has been adopted by Roberts (35) in reviewing the generation of clean surfaces in high vacuum.

Although atomically clean surfaces may be generated in a vacuum of about 10^{-6}, the surface becomes contaminated after a few seconds by residual gases and loses much of its effectiveness. Experiments requiring minutes to hours for completion must be carried out in an ultra high vacuum with pressures on the order of 10^{-9} to 10^{-12} torr. Several methods exist for generating clean surfaces. Some of the more common ones are: glow discharge or ion bombardment (36, 37), heating or baking (38), cleaving and breaking of crystals and glasses (39), and evaporation of a material upon a suitable backing (glass, metal, mica or cleavage faces of crystals) (37). Ion bombardment is highly desirable because of the simplicity of construction of the apparatus and efficiency of cleaning the substrate. However, the method contains a number of disadvantages, e.g., the cleaning takes place at higher pressures

which renders an atomically clean surface impossible, ion cleaning may produce unwanted carbon films by oxidizing carbonaceous materials and pump oils present in the chamber, and finally, metal may be sputtered from the cathode to form what appears to be a clean substrate, but in effect contains a very strongly bonded thin metal film. Cleaning of the substrate by prolonged baking is also a simple procedure. When the substrate is cooled, several monolayers of adsorbed gases may again form, except in ultra high vacuum. Of the above methods mentioned, only cleavage and substrate formation prior to film deposition can provide atomically clean surfaces in the short period of time just before monolayer formation.

d. Substrate interaction

When films are deposited upon substrates with which they can alloy, the interaction is observable as a change in the electron diffraction pattern of the film, a change in the electrical conduction or both. Copper deposited on a gold substrate at room temperature has been found to diffuse immediately into the gold and give a thin skin of copper-gold alloy (29). The alloys which occur at very low temperatures are believed to be the result of high energy vapor atoms diffusing a certain distance into the substrate. At a substrate temperature of 100°C following skin formation, small crystallites of copper form on top of the

Cu-Au alloy. Jeppesen and Caswell (40) have found that lead deposited upon gold formed inter-metallic compounds whose diffraction patterns correspond to $AuPb_2$ and $AuPb_3$. On the other hand, substrates of Ag and Cu are observed to be less effective as prenucleating agents because of no appreciable solubility at either concentration extreme of the Pb-Ag and Pb-Cu phase diagrams. Prenucleated films, in general, become continuous sooner than non-prenucleated ones.

Indium films on glass and quartz may be prenucleated with an intermediate layer of lead deposited between the indium and the glass in a high vacuum (41). However, indium films prepared in this manner have a density of 81% of bulk indium density and a conductivity of only 64% of bulk conductivity.

Since indium mirrors generally indicated films with near bulk properties (38), attempts were made to determine the effects lead had on the conduction of indium films. When the lead layer was thick* enough, the indium film resistance changed with time according to curve 1 in Fig. 1. The magnitude of resistance change was nearly 40% and was found to be typical for

---

*Thickness is given in terms of the frequency change in cycles per second of a quartz crystal monitor, and may be related to "actual thickness" by

$$2\Delta f = dt \qquad 42$$

where Δf is frequency change, d is bulk metal density and t is thickness.

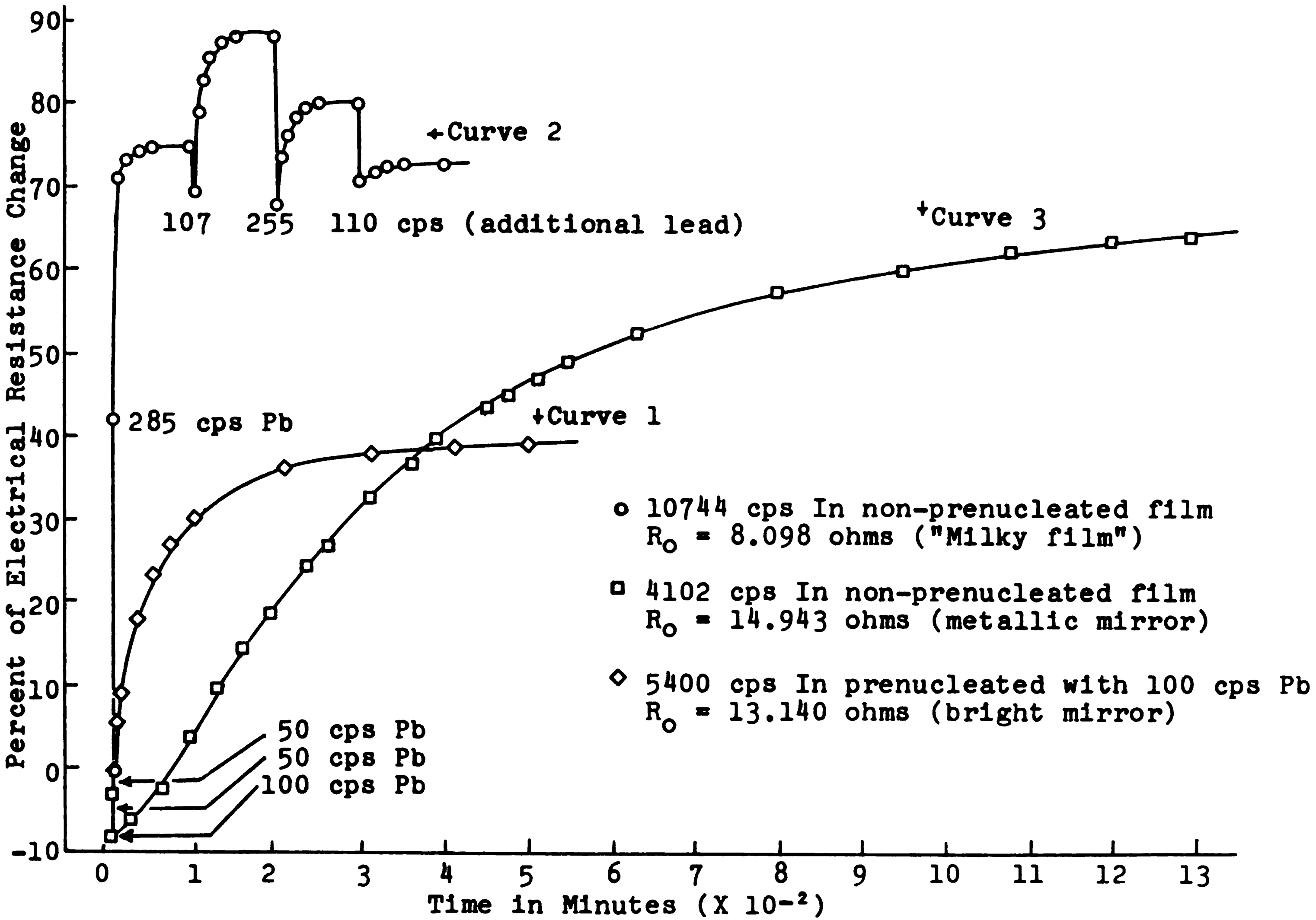

Fig. 1.--Diffusion of lead into indium films.

lead prenucleated indium films. The change was also temperature sensitive and corresponded to Fick's second law of diffusion (42, 43):

$$\partial c/\partial t = D\partial^2 c/\partial x^2 \qquad 43$$

where $\partial c/\partial t$ is the concentration change with time, D is the diffusion constant and $\partial c/\partial x$ is the concentration change with penetration depth, x. Electron diffraction patterns indicated a continuous variation of structure from pure indium to pure lead (see discussion of In-Pb films on page 65). Therefore, as a first approximation, the diffusion constant was independent of concentration (44).

In curves 2 and 3, the sequence of evaporation is reversed to observe the influence of indium film structure (Fig. 2) on the diffusion rate of the lead-indium system. The diffusion constants are determined in accordance with Shaible and Maissel (45), that is,

$$t = d^2/D', \qquad 44$$

where t is the time required for diffusing atom penetration, d is the film thickness and D' the diffusion constant. For curve 2 the diffusion constant is 2.8 x 10^{-13} cm^2/sec, while for curve 3 the diffusion constant is 8.1 x 10^{-16} cm^2/sec, all measurements were taken at room temperature. From these results it is evident that an indium film prenucleated with lead does not furnish realistic data for the pure metal, indium film. Therefore, the use of lead as an atomically clean

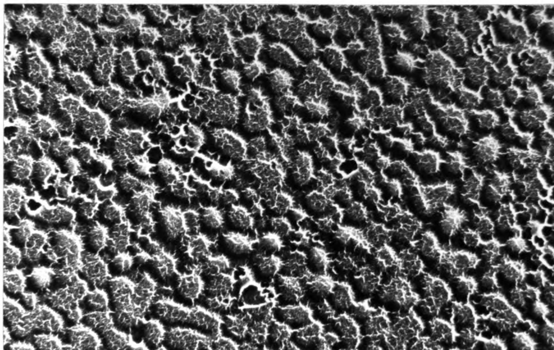

(a)

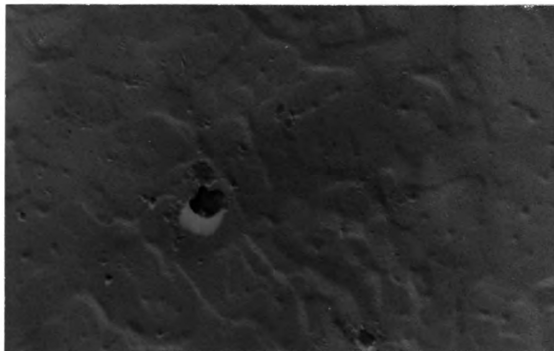

(b)

Fig. 2.--Replicas of indium surfaces prior to lead evaporation, Fig. 1. (a) Surface for curve 2, (b) surface for curve 3. (X 50,000)

substrate is highly questionable. For a more extensive discussion of inter-metallic diffusion in thin films see reference (44).

e. Adsorbed gases on substrates

Substrates prepared in the air and inserted into the vacuum chamber behave quite differently from those prepared inside the vacuum chamber immediately prior to or during the evaporation process. In recent experiments with ionic crystals cleaved in the air and in vacuum, Sella and Trillat (39) found a significant difference in condensation coefficient between the two surfaces. The condensation coefficient, α_c, is the probability that an impinging molecule striking the surface will be "adsorbed, thermally equilibrated, and incorporated (at least temporarily) into the surface in question" (10). For the vacuum cleaved substrate, the condensation coefficient is lower than for the substrate cleaved in air. In addition, the substrate temperature for obtaining an epitaxial film is lower by 125°C to 200°C. The condensation coefficient is affected similarly when glass is broken in vacuum to provide a fresh, atomically clean glass substrate.

2. Vacuum evaporator

Extensive reviews of vacuum technology are currently available which cover a number of basic vacuum

subjects (46, 47, 48) and will not be duplicated to any great extent here.

Metal films formed by evaporation and condensation involve many parameters, some of which have been discussed previously, e.g., substrate temperature, deposition rate and substrate-metal interaction. During evaporation, residual gas impurities are incorporated into the film in proportion to the background pressure. In a vacuum of pressure, P, the number, ν, of residual gas molecules striking the substrate and interacting with the film during preparation, is given by (48)

$$\nu = \tfrac{1}{4} n v_a = \frac{n}{4}\left(\frac{8kT}{m}\right)^{1/2} = P(2\pi mkT)^{-1/2} \qquad 45$$

where n is the molecular density, k is Boltzmann's constant, T is the temperature of the residual gas, and m is the mass of the molecule. The gaseous atom scalar velocity is given by

$$v_a = \left(\frac{8kT}{\pi m}\right)^{1/2} = 14{,}551\left(\frac{T}{M'}\right)^{1/2} \text{ cm/sec}, \qquad 46$$

where M' is the molecular mass of the gas. Therefore,

$$\nu = \frac{14{,}551}{4} n\left(\frac{T}{M'}\right)^{1/2} = 3.5 \times 10^{22} P_{Torr}(M'T_{o_K})^{-1/2} cm^{-2} sec^{-1}. \qquad 47$$

The maximum fractional impurity content due to residual gases (49) is defined as

$$K = \nu/\lambda = 5.82 \times 10^{-2} \; (M/\rho)(M'T)^{-1/2}(P_{Torr}/dT/dt), \qquad 48$$

where ρ is the film density, M is the molecular weight of the metal and dT/dt is the deposition rate. The number of molecules, λ, of film material adhering to the substrate is given by

$$\lambda = \frac{N_o \rho}{M}\left(\frac{dT}{dt}\right), \qquad 49$$

where N_0 is Avogadro's number. Caswell (49) has shown that when the K for oxygen, K_{O_2}, is greater than 3%, the resistivity of indium films evaporated onto a room temperature substrate is 57% higher than bulk resistivity. Below 3% for the maximum impurity content of oxygen, indium films are "metallic mirrors", and below 0.1%, films, which are deposited at a rate corresponding to 100Å/sec and in an oxygen partial pressure of 10^{-7} torr, are found to be indistinguishable from the films prepared in an ultra high vacuum.

Tin films are less sensitive to residual gases; that is, total system pressure may be higher, e.g., 2 to 7 x 10^{-6} torr, and the deposition rate may be lower (86Å/sec) to produce ultra high vacuum-type films (38). However, the importance of residual gases to the final structure of an evaporated metal film cannot be overstressed, and the interaction of metal vapor atoms with residual gases, "gettering", is significant, especially for metals such as In, Ta, Ni and V (50).

B. Methods

1. Vacuum chamber

The vacuum chamber was constructed by Materials Research Corporation and pumped by a 10" oil diffusion pump using DC704 pump fluid, Fig. 3. After an initial bakeout, no further baking was required to obtain a pumpdown time of two and one-half hours, from

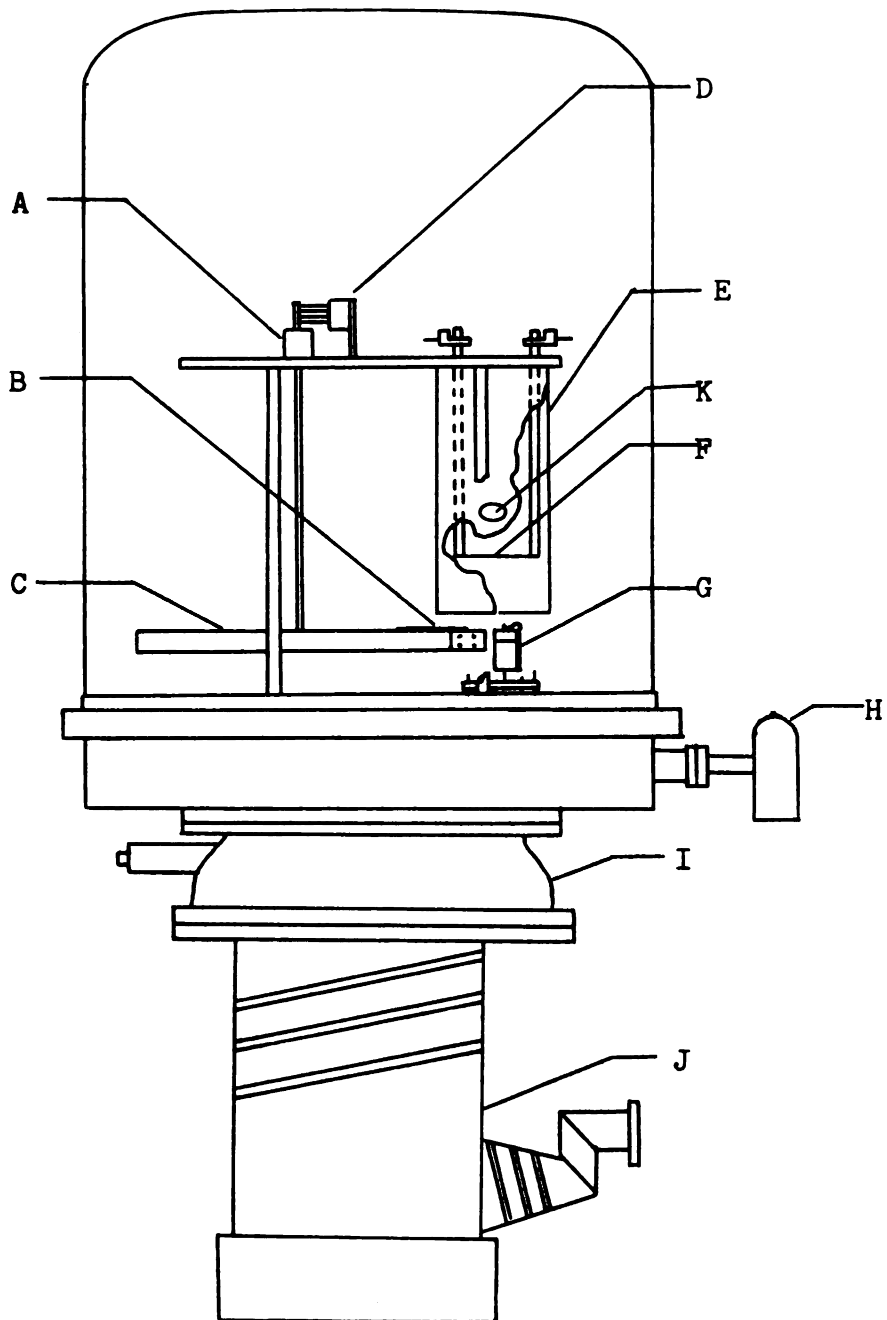

Fig. 3.--Evaporation chamber. (A) Step relay, (B) substrate shutter, (C) counter-balanced substrate turner, (D) slip ring contacts, (E) aluminum shield, (F) molybdenum filament, (G) deposit thickness monitor, (H) ionization gauge, (I) liquid nitrogen baffle, (J) oil diffusion pump, (K) window.

atmospheric pressure to 2×10^{-7} torr. Pressure measurements were made with a Bayard-Alpert type ionization gage which was sufficient to monitor total pressure during the evaporation sequence. The pressure inside the chamber was found to increase from 2×10^{-7} torr to 6×10^{-7} torr during film deposition. The chamber base and cold trap were made of stainless steel, while the bell jar was a standard 18" by 30" glass bell jar which sealed to the base by means of a Viton gasket. Feedthroughs around the base employed Conflat flanges which sealed by the incising action of a double knife edge on a copper gasket (51).

2. Evaporation assembly

The evaporation assembly was suspended from an aluminum plate, which in turn was supported by three 1/2" diameter copper rods. The copper rods were also designed to carry large electrical currents and were bolted to the baseplate for added rigidity. The slip ring contacts provided electrical connections for several functions on the substrate holder, namely, substrate shutter control, thermocouple temperature measurements, substrate heater, and four-point electrical resistance measurements. The step relay, mounted on top of the substrate turner shaft, transported the substrate to one of eight positions for consecutive evaporations. Facilities for three juxtaposed filaments were provided in the suspension plate, while four of the remaining five

positions were not used. The last position was available for glow discharge cleaning and sputtered film preparation. The counter-balanced substrate turning arm changed positions efficiently and smoothly during film deposition. Upon arriving at the desired filament, the turning arm was stopped with an acceptable degeee of precision by the step relay.

The relative positions of the glass substrate, thickness monitor and filament are shown in Fig. 4. The distances from the center of the filament orifice to the centers of glass substrate and quartz crystal monitor are 3 $\pm$ .2 inches, depending upon the final position of the turning arm. The filament has been designed for downward evaporation. To prevent contamination of the different filaments during evaporation, aluminum shields with windows are fastened around the filaments as shown in Fig. 3. The shield windows permit temperature measurements by means of an optical pyrometer. Temperatures obtained from pyrometer measurements are found to agree within 5°C of those measured with a chromel-alumel thermocouple attached directly to the filament.

The substrate holder and mask detail are shown in Fig. 5. The evaporation mask (when used) and substrate are held very securely in position by a small screw in the side of the holder. The outline of the mask permits four-point resistance measurements to be made

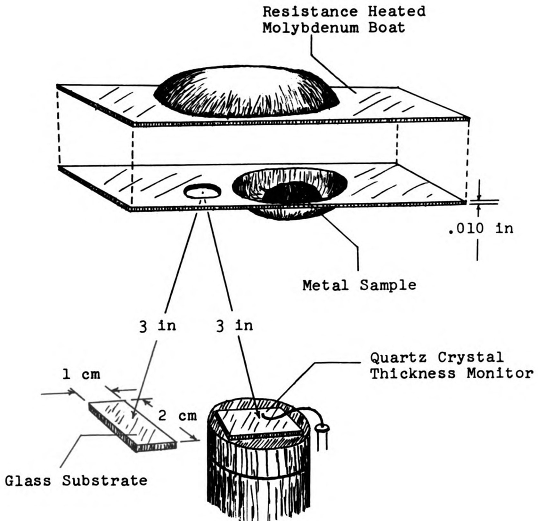

Fig. 4.--Evaporation source and thickness monitor locations.

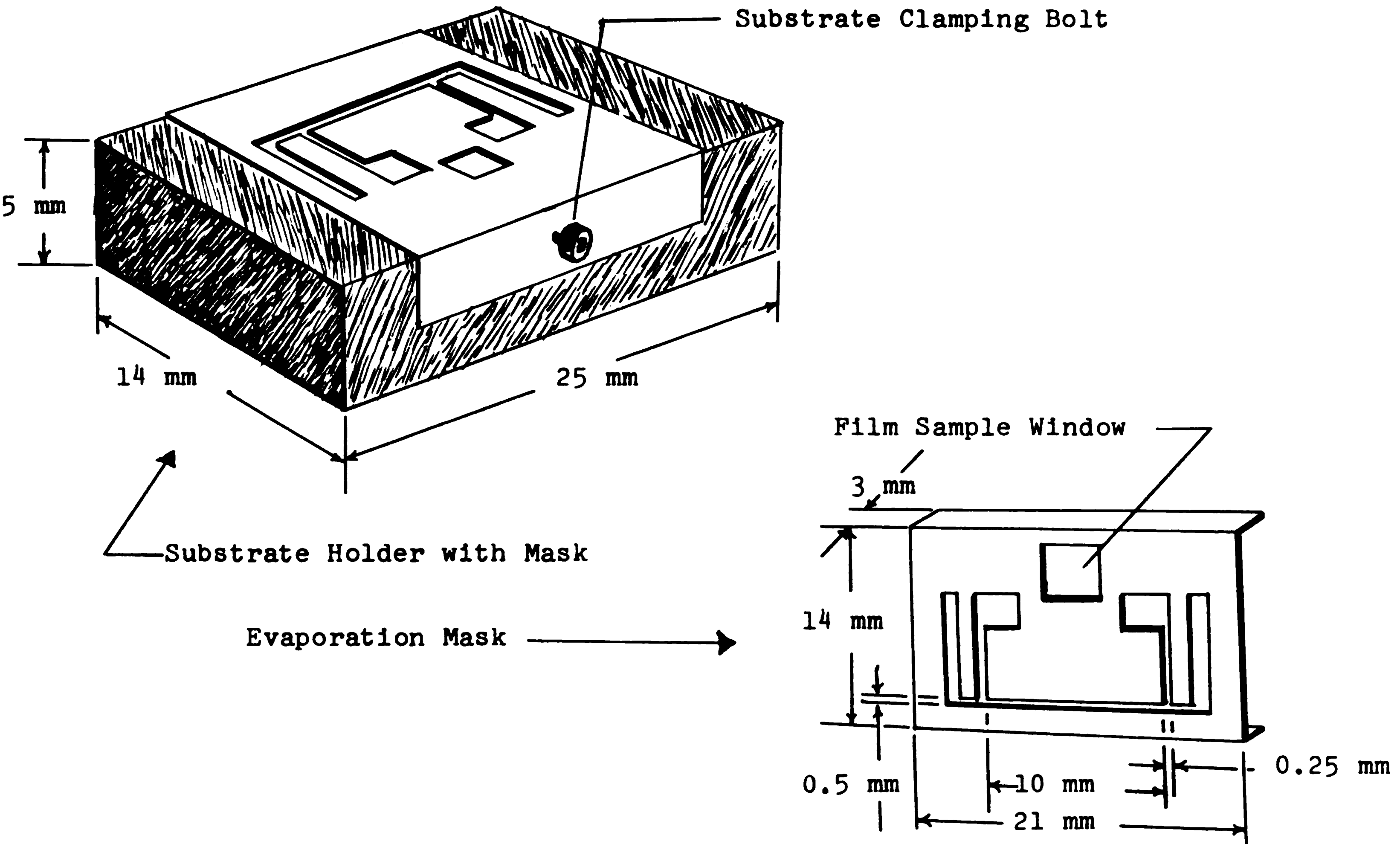

Fig. 5.--Substrate holder and evaporation mask for electrical resistance measurements.

during the evaporation process in the following manner. Prior to film preparation, copper electrodes are evaporated onto the substrate, and No. 30 untinned copper wire loops are inserted between the mask and the electrode. The copper electrodes are located in the upper portion of the substrate and cover the areas outlined by the rectangular posts at either end of the film strip and by the squares whose stems are located 10 mm apart. Film resistance is determined by passing a known direct current through the outer posts and measuring the potential drop across the inner posts. The resistance, R, is then obtained by dividing the potential drop by the current.

The substrate insertion mechanism and shutter are shown in Fig. 6, along with an exploded view of the insertion device. The substrate fits firmly into its holder and is clamped in place by a small screw. Since the arrangement shown here is designed for electron transmission studies of films with varying thicknesses, the evaporation mask in Fig. 5 has been left out. The substrate and holder are then placed into the rotating position adapter and final assembly, adapter and all, is secured in the heating and thermocouple block. Electrical connections, i.e. resistance probes, substrate thermocouple, and substrate heater, are made to the copper plates on the outside of the block. The electrical plates on the block mate with copper brushes inside

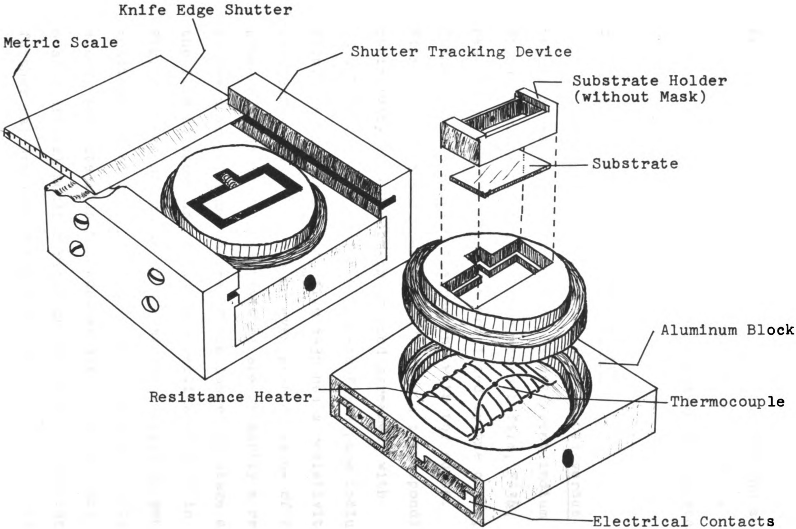

Fig. 6.--Substrate holder, insertion mechanism and shutter.

the shutter tracking device. For final assembly, the heating block is inserted into the shutter tracking device, and the shutter is brought to the edge of the substrate. Parallel alignment of the shutter and substrate allow the location of very thin films to be defined precisely by means of an engraved metric scale on the shutter.

3. Thickness monitor reproducibility

In Fig. 7, film resistances are plotted *versus* thickness monitor readings for six different indium films on glass substrates. The seventh film, F-36, whose resistance and thickness was predicted by the curve, is found to be in excellent agreement with the curve. Film F-30 has a thickness of 2970Å and a corresponding resistivity of 9.0 μohm-cm in good agreement with Caswell's (49) value of 8.9 μohm-cm for a pure indium film. On the other hand, film F-35 has a resistivity of 16.5 μohm-cm and F-32 has an even greater value of 28.7 μohm-cm. The large resistivities are primarily a result of the discontinuous nature of the labyrinth stage of the film as shown in the surface replica of F-35 in Fig. 8. Because indium film resistance based on monitor readings are highly predictable and because, in this study, absolute film thicknesses are not essential, the quartz crystal monitor readings are accepted without further calibration of the instrument. Table 1 presents the data as obtained directly from the monitor with

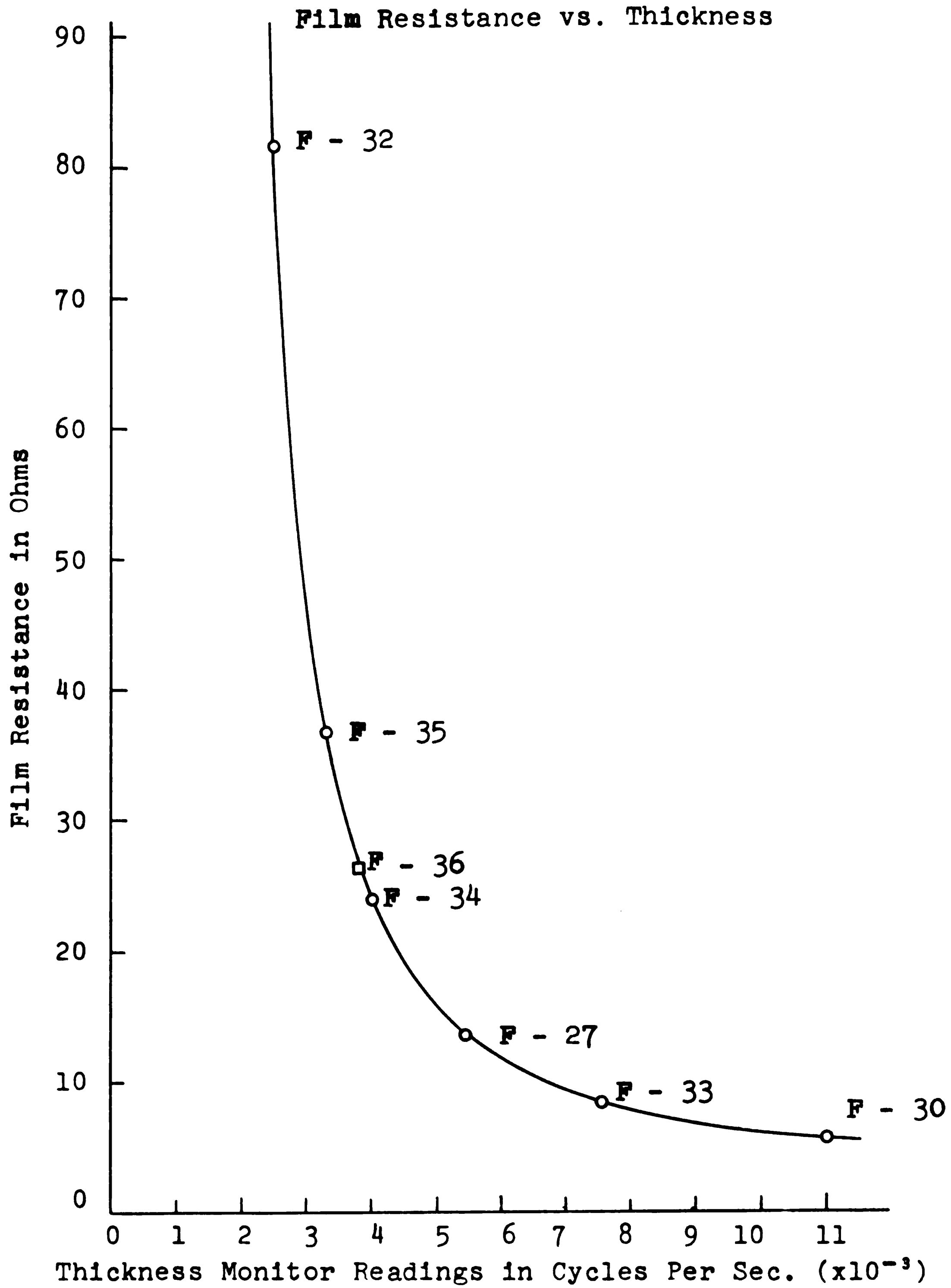

Fig. 7.--Film resistance dependence on thickness for indium deposited on glass.

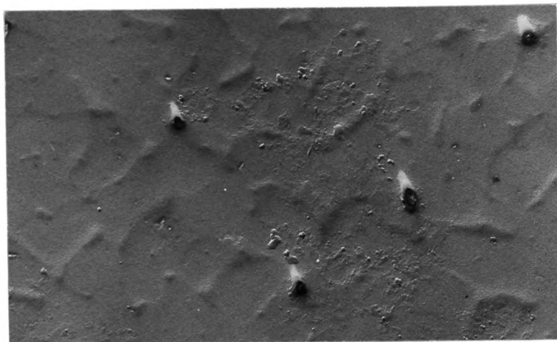

(a)

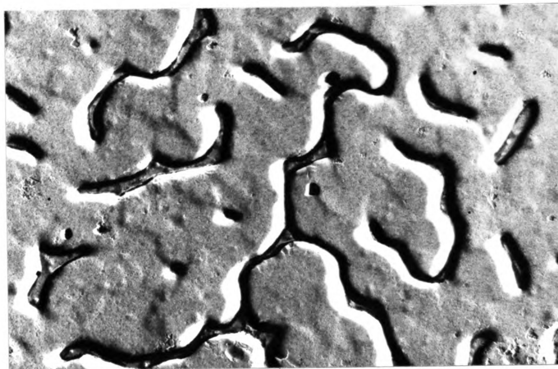

(b)

Fig. 8.--Replicas of indium films for resistance measurements. (a) Film No. F-30, (b) Film No. F-35.

associated deposition times and film resistances. Table 2 contains the film data from Table 1 which has been converted to Ångstroms and resistivities respectively. However, because of the highly discontinuous films which form, a major difficulty occurs in designating film thickness below 1800Å for indium, 700Å for tin and 1100Å for lead deposited upon an amorphous substrate. In lieu of a thickness expressed in units of length, it is suggested here that statements concerning the quantity of material present on the substrate would be less ambiguous. Therefore, film quantities are expressed throughout this paper in cycles per second frequency change of the thickness monitor and may easily be converted to $\mu g\text{-}cm^{-2}$ by multiplying the frequency change by .02.

C. Procedure

1. Filament temperature

Metal films of indium, lead and tin were prepared by evaporating the parent metal from a resistance heated molybdenum filament or boat. The temperature of the filament was measured with a chromel-alumel thermocouple attached directly to the filament and was maintained by manual control of the primary voltage to the high current filament transformer. The filament temperature was found to remain stable during the film deposition, but a slight variation in the line voltage had a pronounced effect on the deposition rate. The curve

TABLE 1

DEPOSIT MONITOR THICKNESS-ELECTRICAL RESISTANCE DATA

Film No.	Monitor Reading (cps)	Deposition Time (sec)	Resistance (ohms)
27	5400	13.2	13.6
30	11000	22.1	5.8
32	2500	6.5	81.7
33	7500	11.1	8.5
34	4000	10.8	24.1
35	3300	7.8	36.7
36	3800	10.1	26.3

TABLE 2

FILM THICKNESS, DEPOSITION RATE AND RESISTIVITY DATA

Film No.	Thickness (Å)	Deposition Rate (Å/sec)	Resistivity (μ ohm)
27	1460	110	10.3
30	2970	135	9.0
32	676	104	28.7
33	2030	183	9.0
34	1080	100	13.5
35	890	114	16.5
36	1035	102	14.0

in Fig. 9 shows the dependence of deposition rate upon filament temperature for indium films.

2. Substrate preparation

a. Glass substrate

From the previous discussion on substrate cleanliness, the importance of having a clean or atomically clean substrate has been demonstrated. Glass substrates used in the electrical resistance measurements were prepared in the way described below. (1) From a standard 1" by 3" Corning glass microscope slide, as many as seven 1 cm by 2 cm substrates could be cut with a diamond glass cutting tool. (2) The glass rectangles were degreased in a sonically vibrated alcohol bath, followed by a brush scrubbing of the surface in a solution of Alconox, a rinsing with deionized distilled water and a final washing with deionized distilled water in the sonic vibrator. The surface was then dried with compressed freon gas. The glass substrates had been found to be very sensitive to skin oils present on the fingers and could not be touched at any time during washing or after final drying. (3) The substrate was then mounted in its holder with mask (see Fig. 5 and 6). When the insertion assemblage was completed, the mechanism was slipped into the shutter tracking device. (4) Electrical connections were completed and tested just prior to chamber closing. (5) After the chamber was pumped to operating pressure,

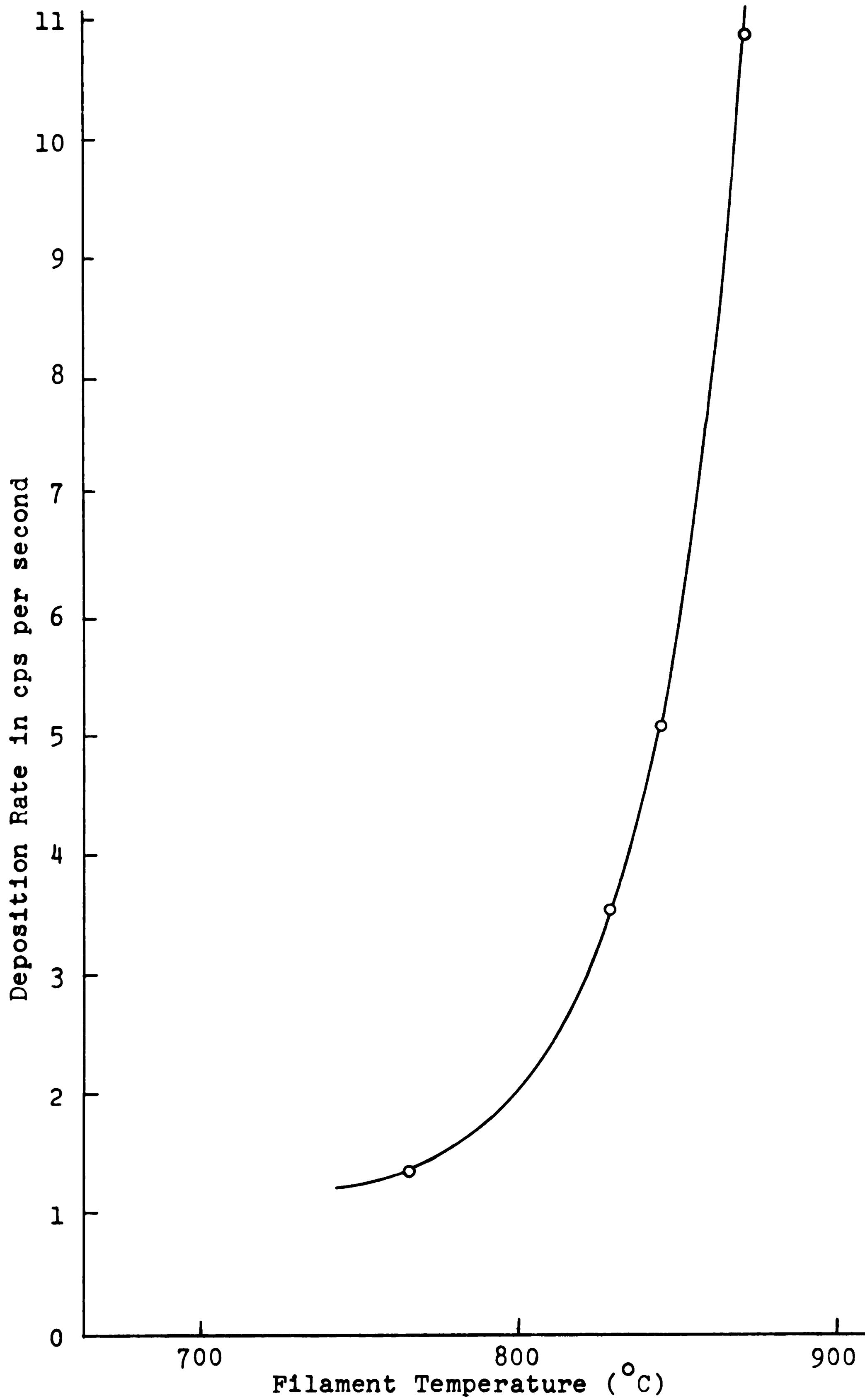

Fig. 9.--Deposition rate dependence upon filament temperature.

2×10^{-7} torr, the glass substrate was baked at 450°C for one hour and allowed to cool overnight. The temperature of the substrate was maintained at 27°C.

b. Silicon monoxide substrate

(1) Air exposure.--Silicon monoxide substrates were prepared by vacuum evaporation of Victawet* from a tungsten filament, followed by evaporation of a small quantity of SiO sufficient to form a continuous amorphous film of about 500Å. At the time the chamber** was brought to atmospheric pressure, the substrate was exposed to air. After the substrate had been prepared, it was installed in the insertion mechanism as described for glass substrates, except that the evaporation mask was not used.

(2) Vacuum prepared silicon monoxide substrates.--Silicon monoxide substrates were prepared immediately prior to metal film deposition and in a manner similar to the substrates just described. However, Victawet and a small quantity of SiO were deposited in the same vacuum chamber as the metal film to be formed. While the substrate was being prepared, the metal filament was pre-heated to give a constant deposition rate

*Victawet is a soap-like material with very low vapor pressure which facilitates removal of the SiO film.

**A second vacuum chamber was used to prepare several silicon monoxide substrates at one time which were stored in a vacuum desicator for future use.

as measured by the thickness monitor. After a sufficient amount of time, and before all the SiO had disappeared from its filament, the step relay (see Fig. 3) was activated and the substrate at the end of the turning arm was immediately exposed to the metal vapor atoms. Substrates prepared in this manner were considered to be atomically clean, since the duration of time for changing the filament was on the order of a few tenths of a second.

3. Film deposition parameter measurements

The duration of film deposition and thickness monitor readings were recorded simultaneously by a Varian x-y plotter. Filament temperature measurements were also noted at various times during the deposition.

4. Electron microscope sample preparation

Microscope samples were prepared from replicas of the film surface or from the silicon monoxide substrates upon which the metal was deposited. Replicas of the metal film surfaces were also made from evaporated silicon monoxide. Following the SiO stripping, the replica was shadowed with platinum to improve the contrast. Water was used as a releasing agent for the SiO film which floated on the surface. The floating film was then lifted from the surface of the water with special microscope grids. (The grids had identification marks for mounting and locating desired portions of the film.)

The silicon monoxide substrate was cut into squares 2 mm by 2 mm with a sharpened needle because that size conveniently covered the 1/8" in diameter microscope grids, and because the shutter was moved across the substrate in integral steps of 1 mm each. Therefore, each film thickness could be located quickly and efficiently.

III. INTERPRETATION OF OBSERVATIONS

A. Indium and lead films

Indium and lead films grown upon amorphous substrates show striking similarities in their growth patterns (Fig's. 10 and 11). Both metals grow in a series of stages beginning with nucleation. During nucleation, nuclei are evenly distributed and of uniform size on the substrate. However, when the migration of adsorbed metal atoms (via surface diffusion) to a stable cluster of atoms is more favorable than the combining with critical nuclei, primary nucleation ceases and the first stage begins. The first growth stage is marked by a dense population of spots, or macula, which are quite uniformly distributed over the substrate. At this time there is little or no fresh nucleation taking place on the substrate and film growth is primarily by surface atom diffusion, except in regions of more concentrated macula. Because of fluctuations in the macula distribution, regions of high concentration may coalesce to form decidedly larger spots. The majority of the macula continue enlarging by surface atom diffusion until they begin touching one another and the first growth stage comes to an end. In the second growth stage, islands develop by coalescing, but because of their spherical cap shape, they grow

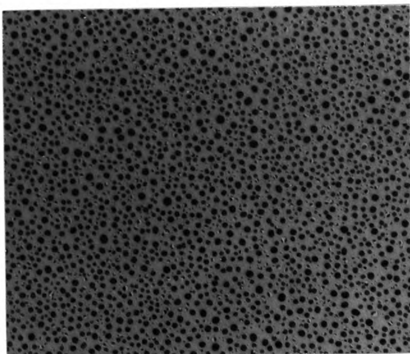

(a)

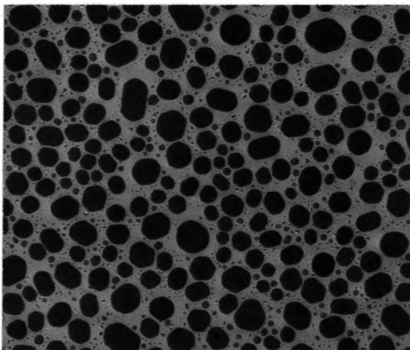

(b)

Fig. 10.--Growth of indium films. (a) 50 cps, (b) 460 cps. (X 40,000)

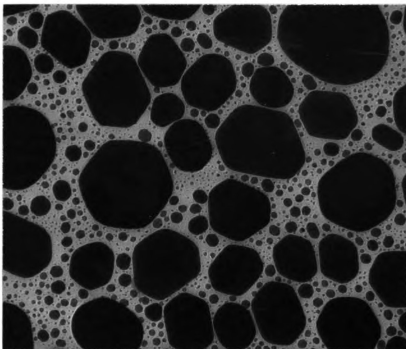

(c)

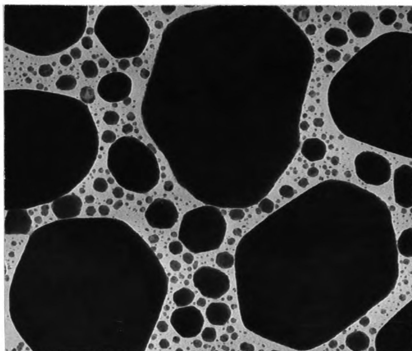

(d)

Fig. 10.--Continued. (c) 1500 cps, (d) 2475 cps. (X 40,000)

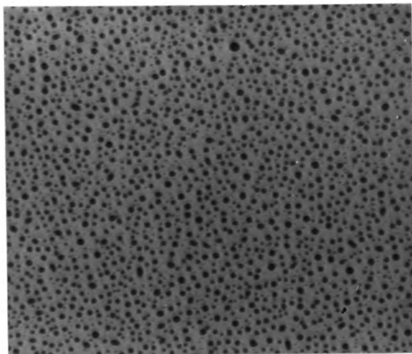

(a)

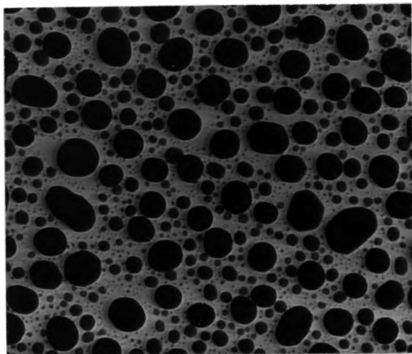

(b)

Fig. 11.--Growth of lead films. (a) 100 cps, (b) 400 cps. (X 40,000)

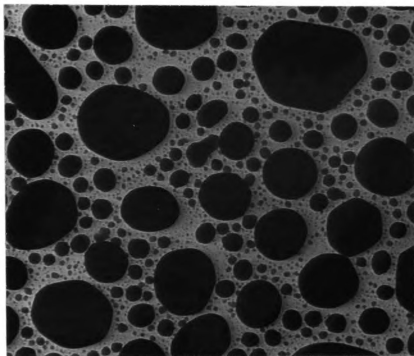

(c)

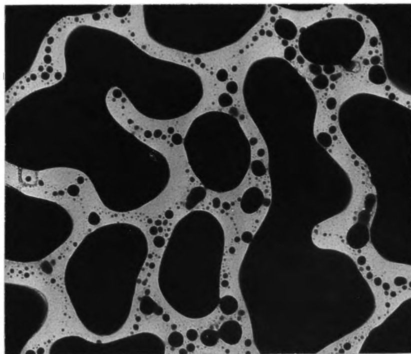

(d)

Fig. 11.--Continued. (c) 1300 cps, (d) 2300 cps. (X 40,000)

three-dimensionally and expose an area of the substrate for nucleation which is greater than the area surrounding the smaller nuclei in the first growth stage. That is, the sum of the area of separate small islands is greater than the area of the large island formed during coalescence. Therefore, during this stage, fresh nucleation occurs.

The third growth stage is artibrarily chosen as the time when the largest island diameter exceeds the smallest observable island diameter by a factor of 30. From this point until the end of the archipelago stage, coalescence of large islands and assimilation of smaller ones are the principle modes of growth. Assimilation is distinguished from coalescence chiefly by the difference in size of the islands involved. Islands of approximately the same size may be said to coalesce, whereas, for the islands of exceedingly unequal proportions, the larger islands assimilate the smaller.

Growth of the islands either by direct addition from the vapor or by addition for surface atom diffusion constitutes the initial and final modes of growth of metal films. Initially the surface area of the islands is small compared to the substrate area surrounding them, and growth by surface atom diffusion predominates. However, at the end of the 'closing' stage of growth, none of the substrate is exposed and the film grows by direct addition from the vapor.

The diffusion distance, X, for a metal atom adsorbed on a substrate may be estimated from electron micrographs by use of the following assumptions; first, an area in which fresh nucleation has taken place, e.g., in very thin films or where nuclei have coalesced and exposed a large substrate area (Fig. 12a), several small uniform spots are visible and mark the location of recently established nuclei. Second, the number of nuclei remains constant from the time of nucleation until they are observed, that is, no coalescence or fresh nucleation occurs. Third, an atom striking the substrate at a distance exactly halfway between two nuclei has an equal probability of migrating to either of them. Fourth, the majority of atoms adsorbed at a distance less than X from a nucleus migrate to it before re-evaporating or colliding with other atoms or molecules to form a critical nucleus. The diffusion distance, X, is given by

$$X = 1/2(A/n)^{1/2}(M)^{-1}, \qquad 50$$

where n is the number of spots in an area, A, on a micrograph with a magnification, M.

Assuming that X remains constant as the spot diameter increases, the area, a', surrounding the spot and having a width equal to the diffusion distance is

$$a' = \pi(r + X)^2 - \pi r^2 \qquad 51$$

$$a' = \pi(2rX + X^2) \qquad 52$$

where 2r is the diameter of the spot.

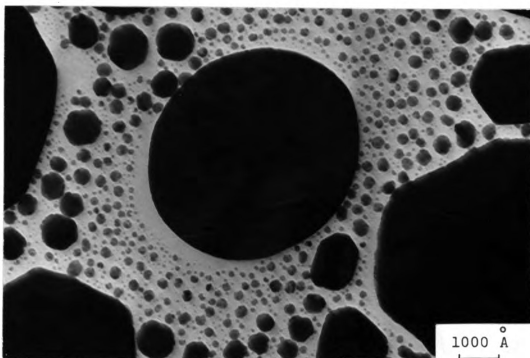

(a)

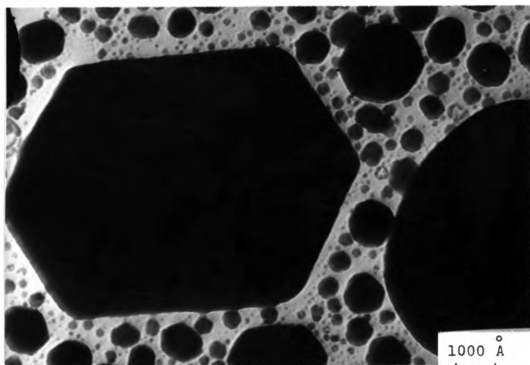

(b)

Fig. 12.--(a) Fresh nucleation on re-exposed substrate following coalescence, (b) hexagonal indium crystallite.

Substituting typical values for X (~100Å) and 2r (~1000Å) in equation 52,

$$a' = 3.46 \times 10^{-11} cm^2. \qquad 53$$

The time dependence of the adatom concentration, dn/dt, is calculated directly from the deposition rate given in units of μg/cm²/sec.

$$dn_1/dt = (N_O/AW)(dm/dt), \qquad 54$$

where AW is the atomic weight of the metal, m is the mass per cm² of metal deposited and N_O is Avogadro's number. For an indium deposition rate of 0.1 μg/cm²/sec,

$$dn_1/dt = 5.25 \times 10^{14} atoms/cm^2 sec. \qquad 55$$

Therefore, if all atoms impingent upon a' are assumed to migrate to the island circumscribed by a', the number, $\tilde{N}_d$, of adatoms added to the island per second is given by the product of the diffusion area and the concentration of adatoms per cm² per sec,

$$\tilde{N}_d = a' \frac{dn}{dt} = \pi(2rX + X^2)(dn_1/dt). \qquad 56$$

At the time when the island diameter is equal to 1000Å, the number of adatoms combining with the island is 18.2 x 10³ atoms/sec. Direct addition to the island from the vapor is the product of the island area and the number of atoms striking the surface of the island per cm² per sec,

$$\tilde{N}_v = dn_1/dt\ (2\pi r^2). \qquad 57$$

Therefore, the number of atoms added to the island is 52.5 x 10³ atoms/sec. It is assumed that the rate of atom addition to the amorphous substrate is the same as

the rate of atom addition to the metal island and that both are equal to the deposition rate as measured by the quartz crystal monitor. This assumption is open to question because of the difference in sticking coefficient, β, is defined as the ratio of atoms which are incorporated into the substrate to the total number of impinging atoms. However, in order to compare the two modes of growth, the coefficients are assumed to be equal.*

The radius of the island as a function of time is related to the number of atoms being added to the island and is given by

$$r = r_o + \left(\frac{3}{2\pi} v_1 t \frac{dn}{dt}\right)^{1/3} \qquad 58$$

where r_o is the radius of the island at t - 1 sec, v is the atomic volume contribution to the island and is taken as the atomic volume of the bulk metal and t is the time of deposition. The geometric shape of the island is assumed to be a hemisphere.

The total number of atoms added to the islands is the sum of the two modes of growth

$$\tilde{N}_t = \tilde{N}_d + \tilde{N}_v = \pi(2rX + X^2) + 2\pi r^2 \, dn/dt. \qquad 59$$

*Since the deposition rate is measured by a quartz crystal coated with the parent metal, the rate obtained is essentially that for atom addition to the metal island. However, the adatom concentration on the amorphous substrate may be related to the deposition rate by

$$dn_1'/dt = \beta_s \, dm/dt \, N_o/AW,$$

where β_s is the ratio of the sticking coefficient for the metal film grown on the bare substrate to the sticking coefficient for the film on the parent metal.

Coalescence in indium and lead films occurs when islands meet and flow together in a liquid drop-like behavior. Infrequently, it is possible to distinguish the general outlines of the two nuclei which form the larger island, but more commonly, the islands tend to be circular. Often a silhouette of the coalescing nuclei remains on the substrate to mark the original positions of the nuclei (Fig. 13). Many nuclei may be involved in forming large islands, as their silhouettes indicate, and it appears that some islands travel great distances across the substrate. It is characteristic for indium films to form geometrically shaped islands as shown in Fig. 12b. Generally, the islands are hexagonal, very seldom pentagonal, but never, in all the observations, has the number of sides exceeded six nor been less than five. The hexagonal crystal habit of islands has been found in indium films whose thickness ranges from 750-2000 cps. Prior to 750 cps the island shape is roughly circular, while after 2000 cps the larger islands are somewhat irregular. However, films greater than 2000 cps contain some hexagonally shaped islands which are comparable in size to the islands found in the 750 to 2000 cps range. The crystal habit varies from island to island and may be related to the manner in which the island grows. The sequential micrographs in Fig's. 14 and 15 show the evaporation of indium nuclei during exposure to the electron beam in the microscope. It is obvious from Fig. 14 that many of

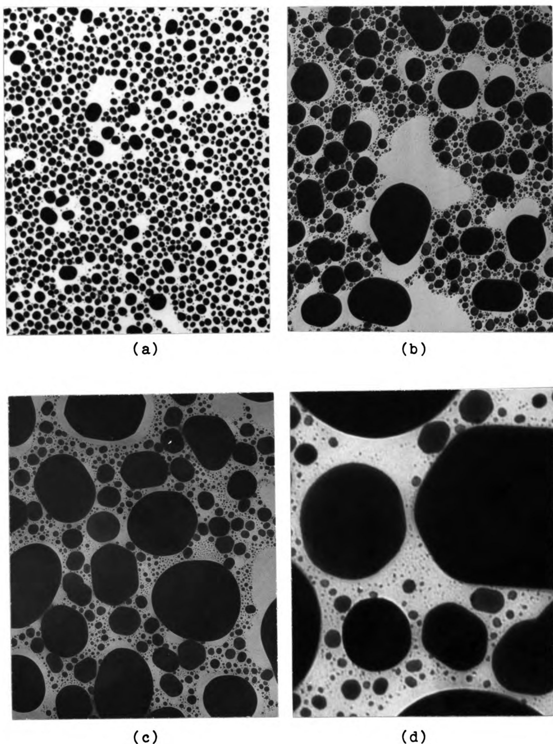

Fig. 13.--"Milky" indium film. (a) 300 cps (X 20,000), (b) 1334 cps (X 20,000), (c) 2630 cps (X 10,000), (d) 2630 cps enlargement of (c) at (X 40,000).

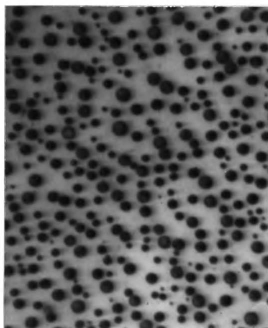

(a)

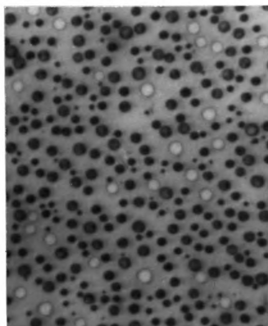

(b)

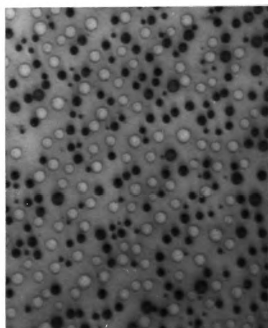

(c)

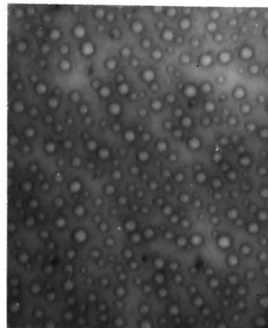

(d)

Fig. 14.--100 cps of indium evaporated by the electron microscope beam during observation. (a) 0 sec, (b) 10 sec, (c) 20 sec, (d) 40 sec. (X 100,000)

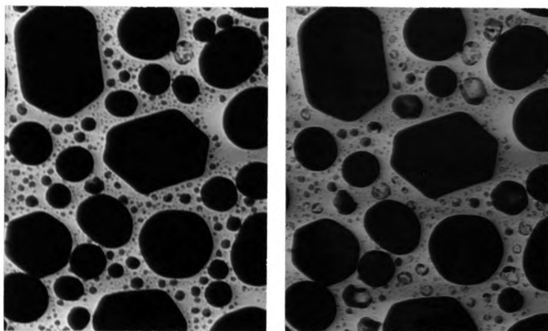

(a) (b)

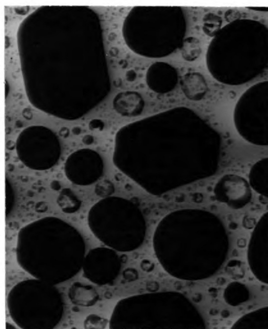

(c)

Fig. 15.--750 cps indium film evaporated by the electron microscope beam. Note small spots under large evaporated islands. (a) 0 sec, (b) 10 sec, (c) 15 sec. (X 35,000)

the larger nuclei evaporate before the smaller ones. On close examination of the micrographs, the larger nuclei appear to be thinner than the smaller ones, which suggests that the nuclei thickness changes during the initial growth period from a spherical cap to a round platelet. Therefore, evaporation due to heat generated by the electron beam would be greatest for the large surface to volume ratio for the platelet. It is difficult to explain the island traces left on the substrate as shown in Fig. 14d, however, it is believed that some metal remains firmly bonded to the substrate and disappears only after prolonged exposure to the beam. The evaporation sequence in Fig. 15 upholds the explanation for metal remnants on the surface. In the micrograph an island near the top center has evaporated and left a shell. A similar shell was observed to be three-dimensional, that is, during examination of the same microscope grid as appears in Fig. 19, one of the spots on the edge of the substrate evaporated and left a protruding structure. A possible explanation for the evaporation of large islands is suggested by the appearance of small spots under the shells. Generally, when islands coalesce (see Fig. 13 or the round spot at right center in Fig. 15), large areas of the substrate are left completely devoid of small nuclei. This phenomenon appears to be contrary to the evidence obtained from the evaporation sequence micrographs which

clearly show that small nuclei under the larger islands still maintain their identity. Therefore, at least two types of island formation are observed: one type forms as a result of coalescence and is fairly stable, while the other appears to grow from seed crystals on the substrate and is relatively unstable. The islands grown from seed crystals extend into space connected to the substrate by the seed crystal, and it is not uncommon to find larger islands extending out over smaller ones with no apparent interaction.

B. Tin films

The initial stages of growth for tin films are similar to indium and lead, that is, following nucleation the concentration of nuclei is large and their size is somewhat uniform. Coalescence, however, is quite different in several aspects (Fig. 16). The largest islands are somewhat immobile and very thin as compared to indium or lead. Also, the arrangement of smaller islands within the larger ones is clearly visible because the joining edges assume the appearance of well defined grain boundaries. There is no tendency for the islands to flow together, and therefore they maintain a separate identity even in the advanced labyrinth stage. The islands are nearly two-dimensional in comparison with indium islands with the same quantity of metal deposited. Because of the two-dimensional growth,

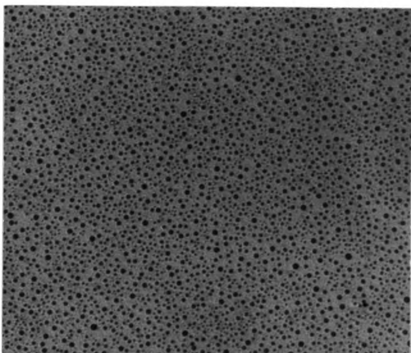

(a)

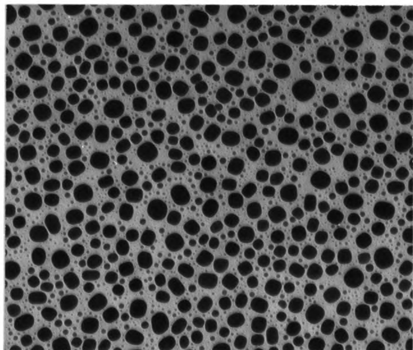

(b)

Fig. 16.--Growth of tin film. (a) 30 cps, (b) 400 cps. (X 40,000)

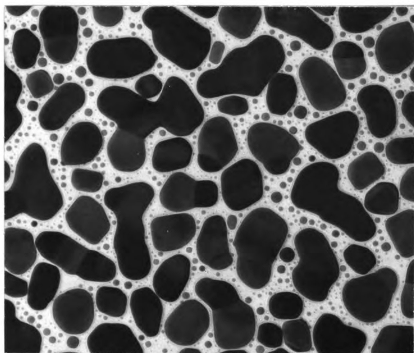

(c)

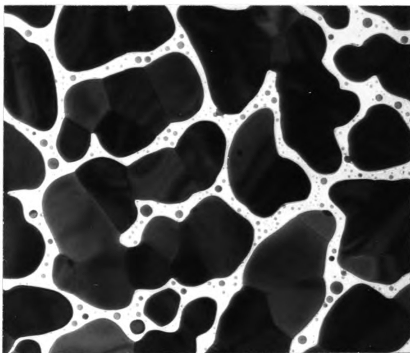

(d)

Fig. 16.--Continued. (c) 970 cps, (d) 1340 cps. (X 40,000)

the labyrinth stage occurs earlier and accordingly, the continuous film which forms is much thinner.

C. Indium-lead films

The growth of indium on lead films differed somewhat from the growth of indium films alone. The two basic island shapes observed in the films were hexagonal and oval. The number of hexagonally shaped islands was fewer than for those of indium alone, and the number of oval islands was considerably larger. Fig. 17 shows the growth of indium on 100 cps of lead. In Fig. 17d, a large amount of fresh nucleation has just occurred and, moreover, small intermediate sizes are conspicuously absent. Comparing this film growth with that for indium alone, Fig. 10c, the distribution of island sizes differs significantly. The even distribution and fairly uniform size of the fresh nuclei in the indium-lead films are probably pure indium.

The diffraction patterns in Fig. 18 are for (a) pure lead, (b) pure indium, (c) lead plus indium with a 1:1 mass ratio for a thicker film. The pattern in Fig. 18c occurs only for a 1:1 mass ratio and only when the film is very thin. Note, however, that its mass is not less than the masses for the pure metals which give well defined lines in their respective patterns. Also, the large bright line in Fig. 18c occurs between the lead line with a d-spacing of 1.750 and an indium line with a d-spacing of 1.683. The diffused nature of the pattern

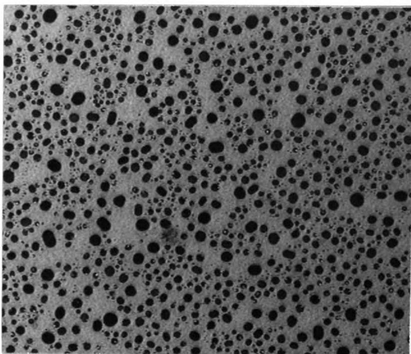

(a)

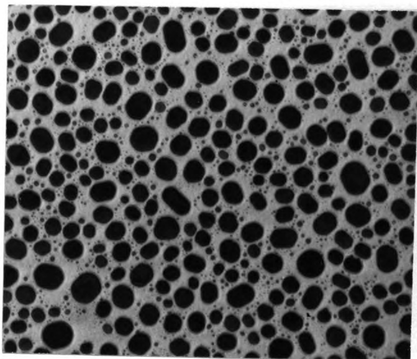

(b)

Fig. 17.--Indium film grown on 100 cps lead. (a) 240 cps, (b) 435 cps. (X 40,000)

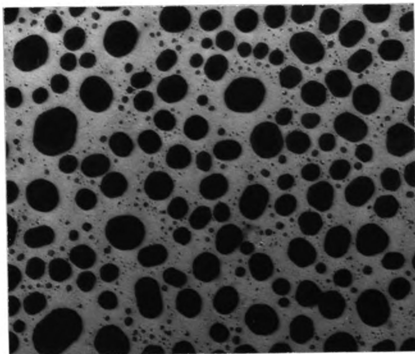

(c)

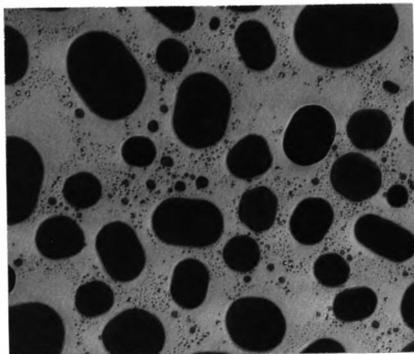

(d)

Fig. 17.--Continued. (c) 750 cps, (d) 1100 cps. (X 40,000)

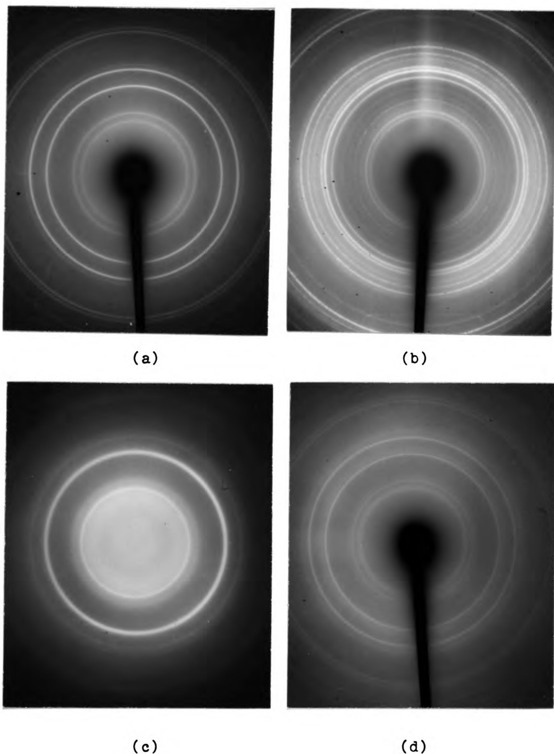

Fig. 18.--Electron diffraction patterns. (a) Pure lead with monitor thickness of 75 cps, (b) pure indium thickness 75 cps, (c) indium plus lead, 75 and 75 cps thicknesses respectively, (d) indium plus lead, 150 and 150 cps respectively.

suggests that the lead-indium alloy formed varies continuously from pure indium to pure lead. The thickness of the alloy layer is limited, and excess lead and indium give the superimposed diffraction patterns shown in Fig. 18d. When the concentration of one metal is greater than the other, only the diffraction pattern for the predominant metal is observed.

D. Contact angles

The study and measurement of the contact angle between a metal and its substrate usually involves melting a metal bead on the substrate, cooling the substrate to ambient temperature, and sectioning and photographing the metal bead (8). The metal bead is mounted in a transparent resin after it has cooled on the substrate, and care must be exercised during sectioning to insure the desired bead cross section. In the electron microscope, however, a 'three-dimensional' micrograph of indium on silicon monoxide reveals not only the contact angle of several islands, but also the relative island thicknesses. For indium, the contact angle varies from 80° to 90°.

'Three-dimensional' micrographs were obtained when the grid mounted substrate developed a small crack which tore the full length of the grid opening. While the substrate was still in the beam of the electron microscope, the edges along the crack curled and folded under.

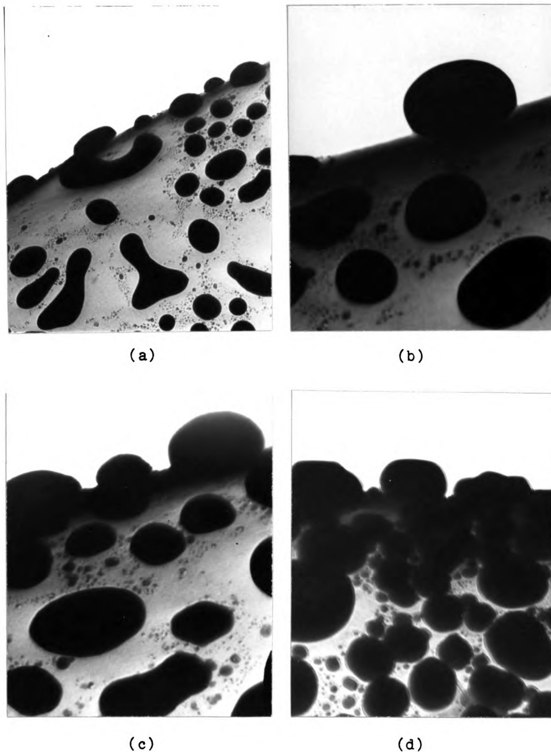

Fig. 19.--Three-dimensional electron micrographs of metal films on silicon monoxide substrates. (a) Indium (X 20,000), (b) lead (X 60,000), (c) lead plus indium (X 60,000), (d) "Milky" indium film (X 50,000).

When too much folding took place a 'double exposure' resulted and island attachment to the substrate was difficult to locate. Therefore, the most satisfactory micrographs were obtained in the region near the ends of the crack where the substrate was supported by the grid.

The angle between the substrate and island is measured between a line tangent to the point of contact with the substrate and a line parallel to the base of the island. In some instances, such as in Fig. 19b, the island is tilted out of the page so that the mid-point on the base must be estimated for purposes of drawing a line parallel to the base. For lead, the contact angle is estimated to be 85° to 95°; for lead plus indium, it is 90°; and for the 'milky' indium film it is 120°.

Contact angles for tin were not obtained because of the very thin and tightly bonded metal islands which apparently prevented the substrate from cracking. It was observed in the cases mentioned above that as the substrate pulled apart, the islands across the developing crack remained attached to one side or the other and appeared to be suspended in space.

IV. ANALYSIS AND RESULTS

A. Analysis

Several indium films and one each of lead, tin and lead plus indium were prepared by thermal evaporation upon silicon monoxide substrates. Some of the indium, the lead and the indium plus lead films were produced on substrates prepared in a separate vacuum chamber, exposed to the atmosphere, baked in the primary evaporation chamber and, finally, cooled to ambient temperatures. The rest of the indium films and the tin film were formed on fresh silicon monoxide substrates prepared *in situ*. After proper mounting of the film and substrate on microscope grids by the standard flotation method, the sample was inserted into the electron microscope and examined. Several sections of the grid were investigated to determine the most representative areas of that portion of the film. Following the selection of desired area, micrographs were made at a primary enlargement of (X 35,000). Prints were made at a secondary enlargement of (X 140,000) and were found to be superior to the prints of the same secondary enlargement but a different primary enlargement of (X 70,000). At (X 70,000) the electron beam intensity was great enough to cause small island vaporization and thereby severely disrupt focusing procedures.

When satisfactory micrographs are ready for analysis, each print contains islands of various sizes which are measured and counted. The fraction of coverage is given by

$$a_i/a_c = \text{fractional coverage}, \qquad 60$$

where a_i is the total area covered by the number of islands, i, of the same size and a_c is the area over which the count is made. For convenience of calculation, all islands are assumed to be circular and all diameter measurements for the same film are made with a ruler perpendicular to one edge of the micrograph. For any given area at least fifty islands of the same size are assumed to constitute a representative sample of the film, and although numbers of islands less than fifty were often counted, they were still included in the analysis for estimation purposes.

The curves obtained by plotting the data and connecting each point with a smooth line serve only to indicate the trend in film growth and are not intended to indicate numbers of intermediate sized islands.

B. Results

1. Indium film No. 1--deposition parameters

Deposition rate	10.88 cps/sec
Substrate temperature	Ambient
Filament temperature	869°C
Background pressure	6 x 10^{-7} torr

TABLE 3

OCCURRENCE OF PREDOMINANT PEAKS FOR INDIUM FILM NO. 1

Quantity of film material	Location of peaks
845 cps	3, 8, 10, 24, 31, 35, 40, 45, 48, 50, 53, 56, 60
610 cps	5, 10, 20, 23, 25, 30, 35, 40, 45, 50, 53
458 cps	5, 15, 17, 20, 25, 30, 34, 38, 40
290 cps	5, 11, 13, 15, 17, 20, 23, 25
146 cps	3, 9, 13
53 cps	6

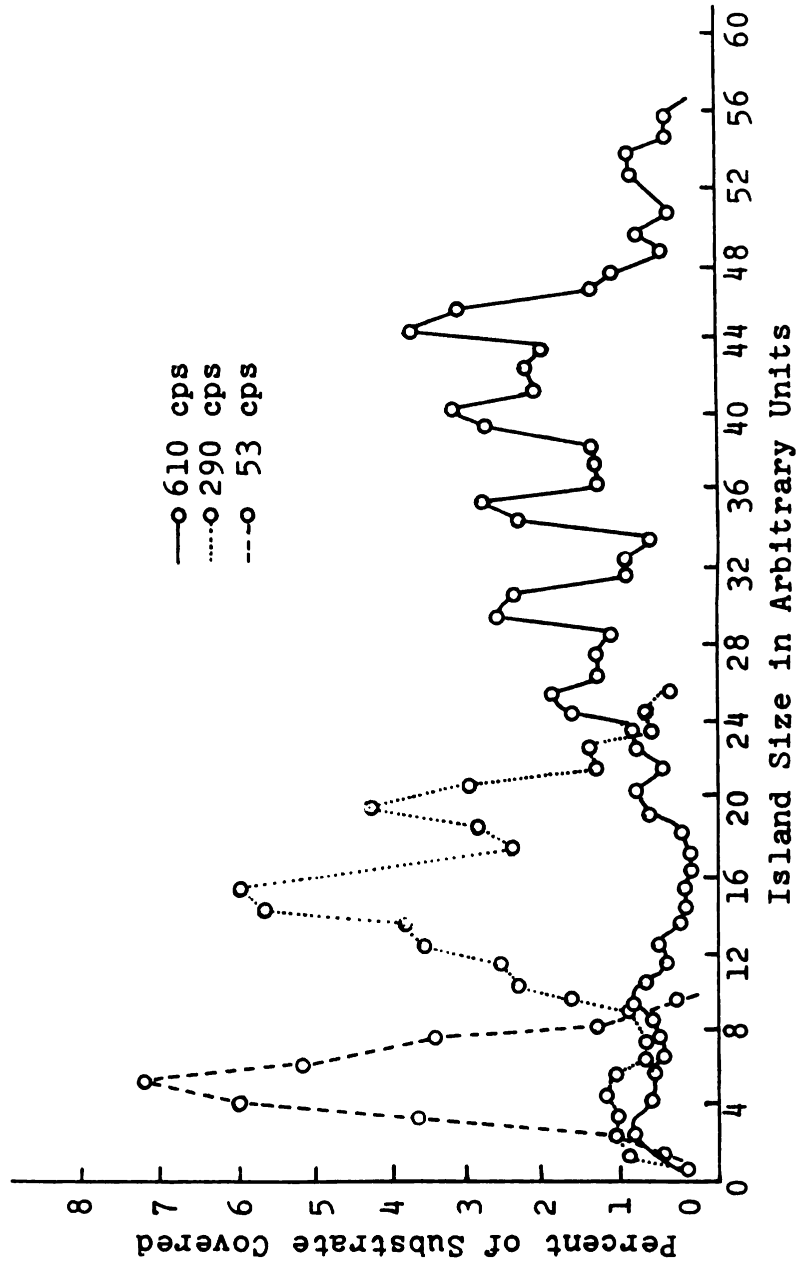

Fig. 20.--Indium film No. 1. Indium deposited upon SiO prepared *in situ*.

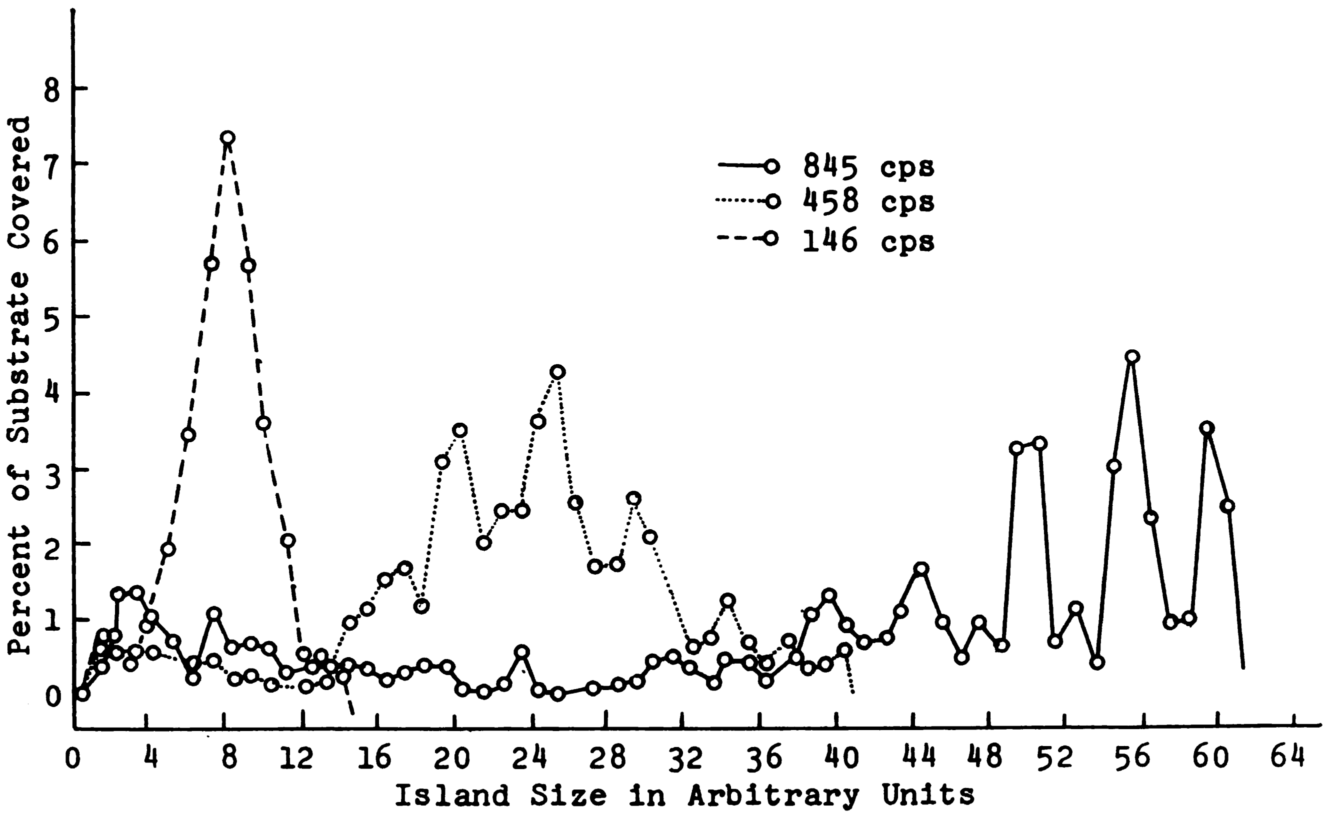

Fig. 20.--Continued.

2. Indium film No. 2--deposition parameters

Deposition rate	5.13 cps/sec
Substrate temperature	Ambient
Filament temperature	845°C
Background pressure	6×10^{-7} torr

TABLE 4

OCCURRENCE OF PREDOMINANT PEAKS FOR INDIUM FILM NO. 2

Quantity of film material	Location of peaks
750 cps	2, 10, 15, 20, 25, 30, 35, 37, 40, 45, 48, 50, 52, 55, 60, 64
487 cps	3, 5, 10, 15, 20, 25 27, 33
266 cps	3, 10, 14, 20
90 cps	3, 5, 7

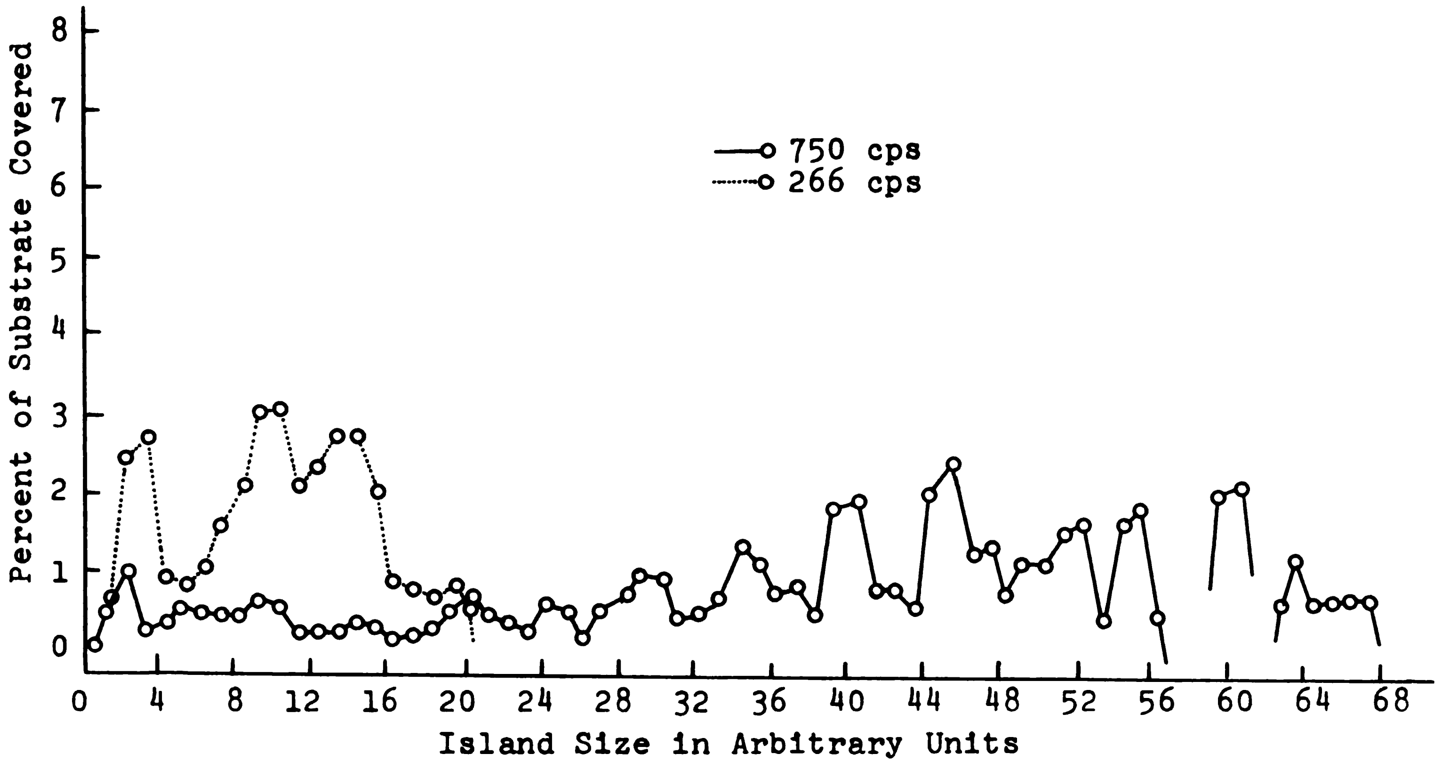

Fig. 21.--Indium film No. 2. Indium deposited on SiO prepared *in situ*.

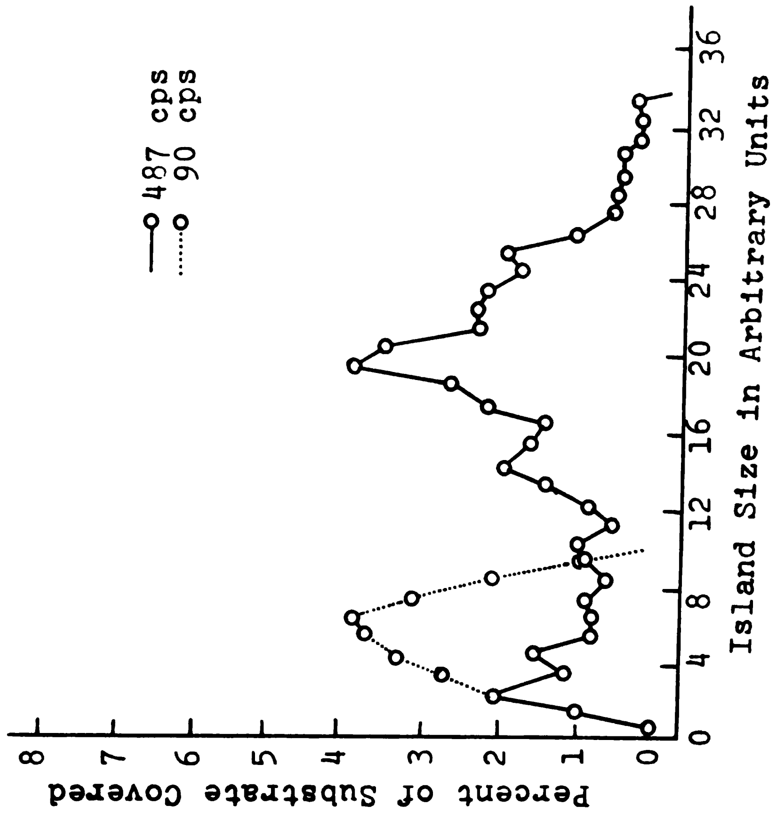

Fig. 21.--Continued.

3. <u>Indium film No. 3--deposition parameters</u>

Deposition rate	1.70 cps/sec
Substrate temperature	Ambient
Filament temperature	766°C
Background pressure	6×10^{-6} torr

TABLE 5

OCCURRENCE OF PREDOMINANT PEAKS FOR INDIUM FILM NO. 3

Quantity of film material	Location of peaks
454 cps	2, 3, 11, 15
381 cps	2, 5, 10, 13
244 cps	5
154 cps	3

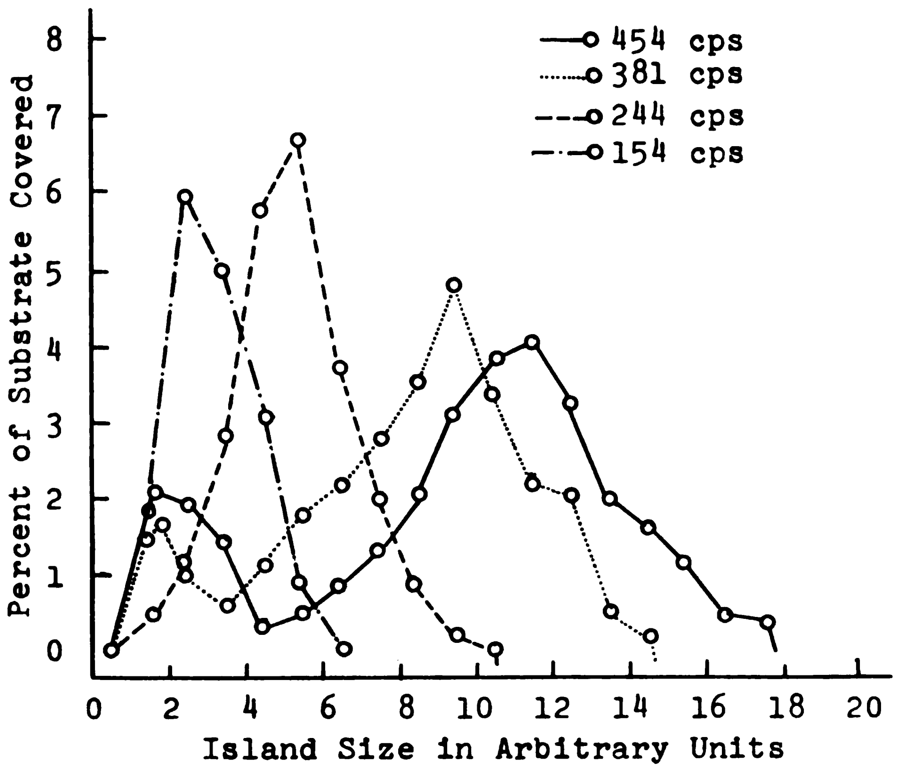

Fig. 22.--Indium film No. 3. Indium deposited on SiO prepared in a separate chamber.

4. <u>Indium film No. 4--deposition parameters</u>

Deposition rate	5.13 cps/sec
Substrate temperature	Ambient
Filament temperature	845°C
Background pressure	6 x 10^{-7} torr

TABLE 6

OCCURRENCE OF PREDOMINANT PEAKS FOR INDIUM FILM NO. 4

Quantity of film material	Location of peaks
648 cps	3, 7, 20, 25, 27, 30, 32, 40, 47, 50, 56
432 cps	3, 7, 11, 13, 15, 20, 23, 25, 30
242 cps	8, 10, 12
62 cps	3, 6

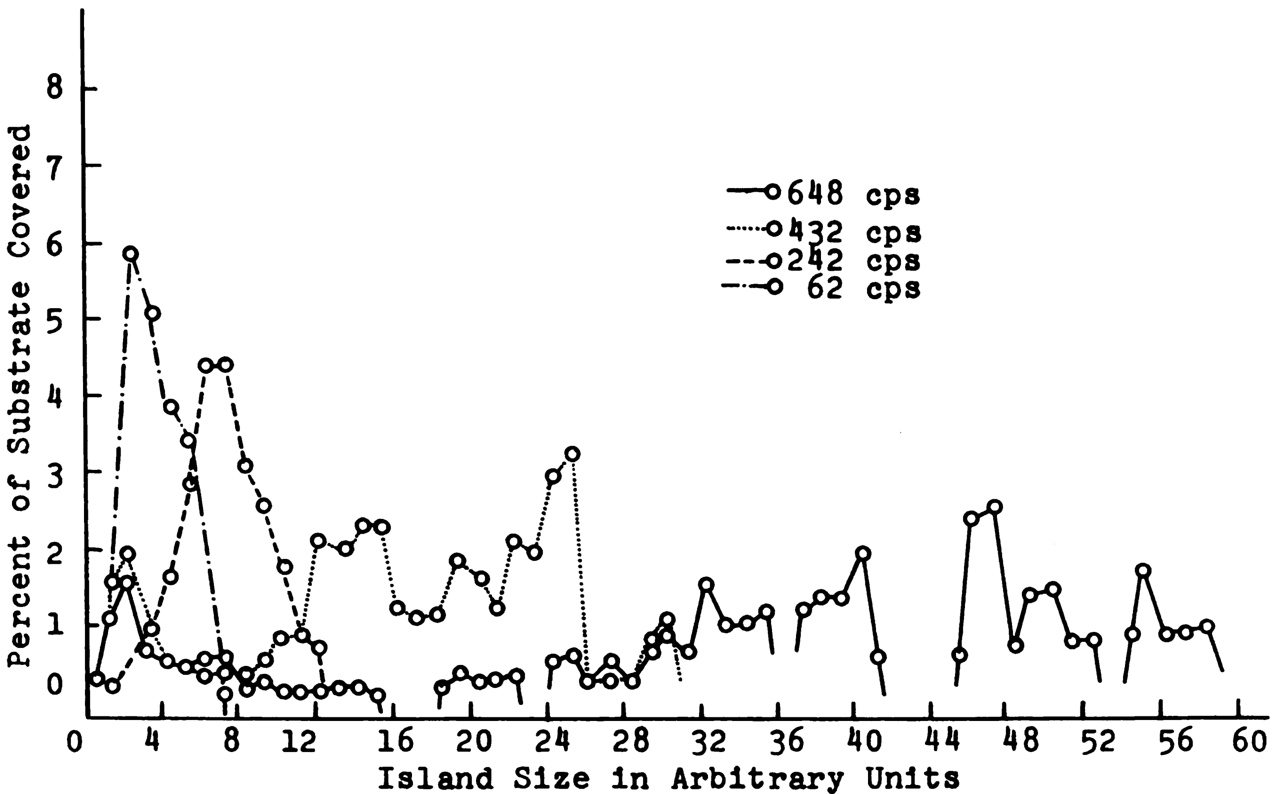

Fig. 23.--Indium film No. 4. Indium deposited on SiO prepared in a separate chamber

5. Lead film--deposition parameters

Deposition rate	7.41 cps/sec
Substrate temperature	Ambient
Filament temperature	
Background pressure	1 x 10^{-6} torr

TABLE 7

OCCURRENCE OF PREDOMINANT PEAKS FOR LEAD FILM

Quantity of film material	Location of peaks
400 cps	3, 7, 11, 13, 15, 18, 20, 23, 25
300 cps	4, 10, 13, 15
150 cps	2, 4, 7
75 cps	2

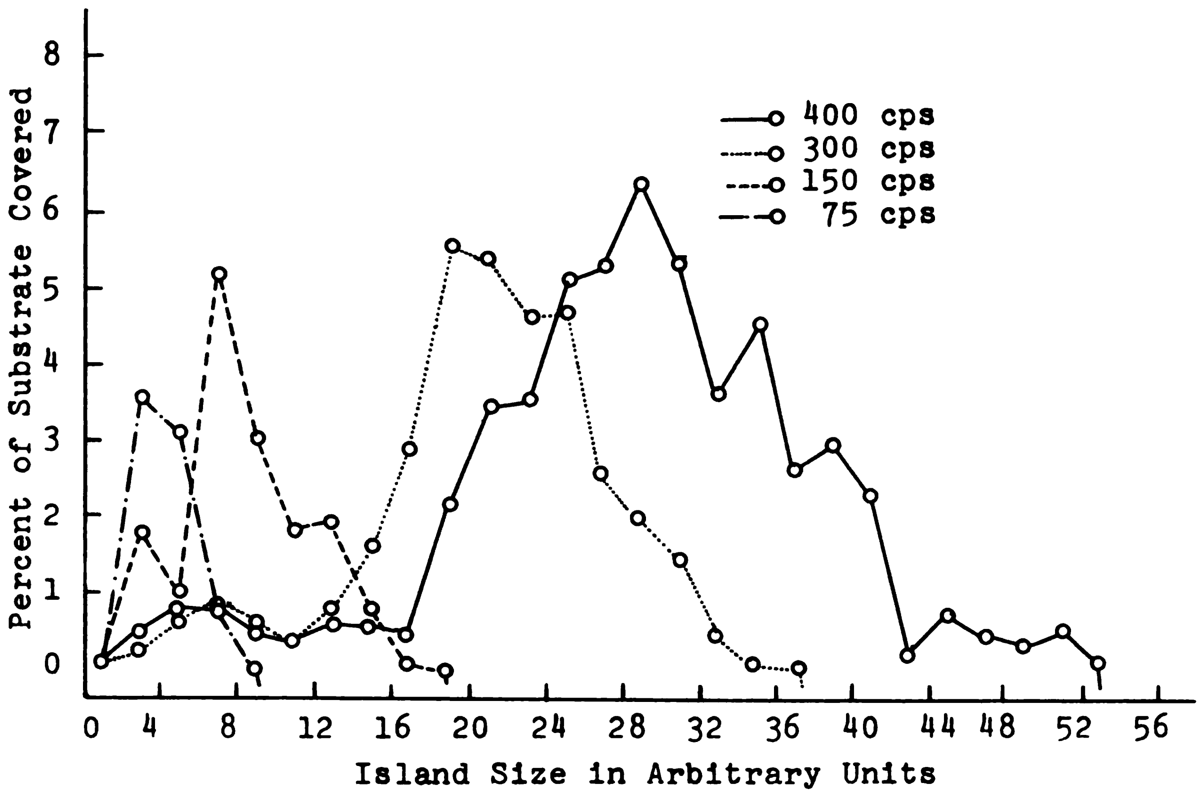

Fig. 24.--Lead film grown upon SiO prepared in a separate chamber.

6. Tin film--deposition parameters

Deposition rate	2.35 cps/sec
Substrate temperature	Ambient
Filament temperature	1750°C
Background pressure	2 x 10^{-6} torr

TABLE 8

OCCURRENCE OF PREDOMINANT PEAKS FOR TIN FILMS

Quantity of film material	Location of peaks
988 cps	Not computed
617 cps	3, 8, 10, 16, 18, 20, 23, 25, 28, 30, 32, 35, 38, 40
400 cps	4, 15, 18, 23
191 cps	3, 10, 13, 15, 17
88 cps	3, 5, 10, 13
32 cps	5

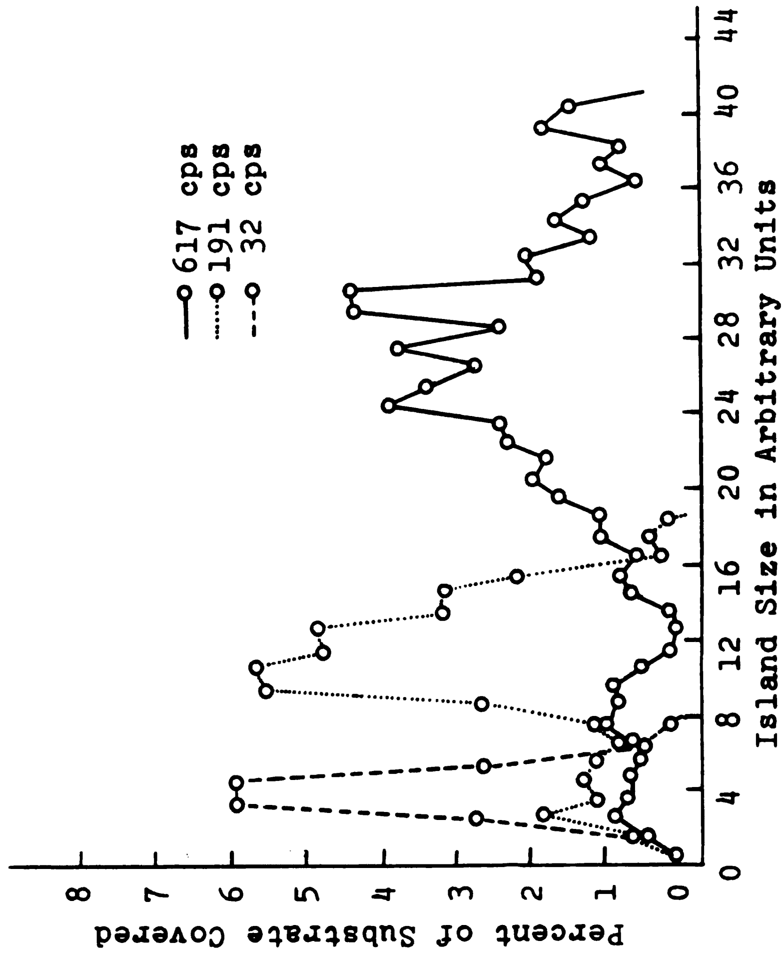

Fig. 25.--Tin film grown upon SiO prepared <u>in situ</u>.

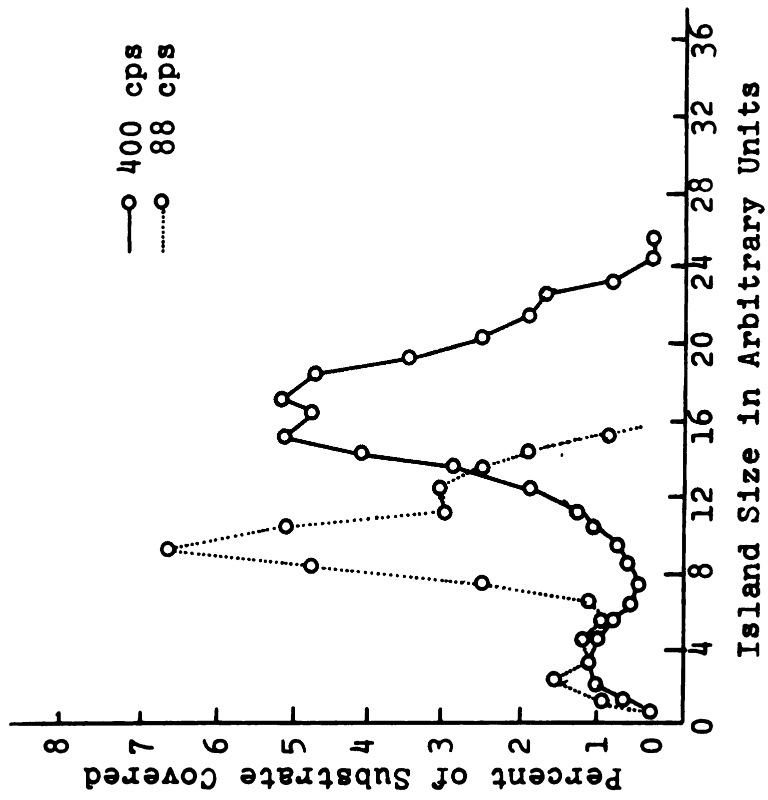

Fig. 25.--Continued.

7. <u>Indium film on lead--deposition parameters</u>

Deposition rate	5.75 cps/sec
Substrate temperature	Ambient
Filament temperature	855°C
Background pressure	1 x 10^{-6} torr

TABLE 9

OCCURRENCE OF PREDOMINANT PEAKS FOR INDIUM FILM ON LEAD

Quantity of film material	Location of peaks
750 cps	2, 6, 16, 20, 24, 25, 28, 30, 35, 40, 46
607 cps	2, 10, 15, 20, 21, 25, 28, 29
470 cps	2, 8, 10, 11, 13, 16
240 cps	2, 6, 8, 10

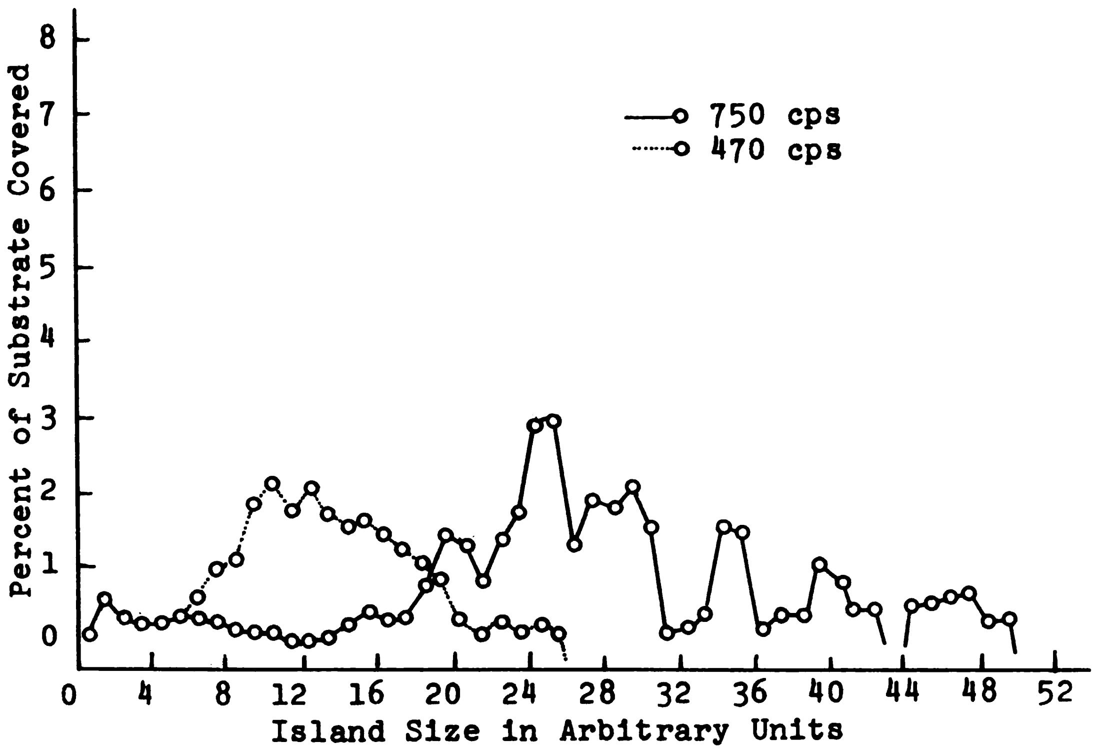

Fig. 26.--Indium deposited upon 100 cps of lead.

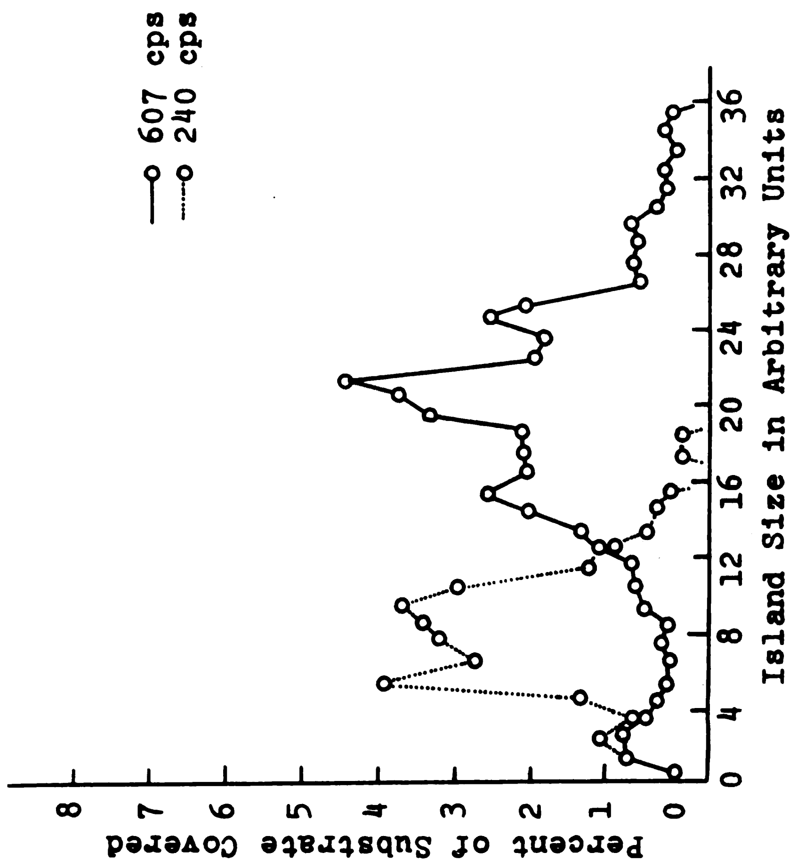

Fig. 26.--Continued.

V. CONCLUSIONS

1. The results of the study indicate that during the nucleation and archipelago growth stages for indium, lead and tin films, a secondary series of stages occurs. After nucleation the film grows first as a collection of densely populated, non-interacting islands, second by coalescence of intermediate sized nuclei to form larger islands, and third by coalescence of large islands and by assimilation of small nuclei by larger ones.

2. During the initial growth, films are composed of relatively uniform islands whose size is a function of the quantity of metal deposited. In later stages of growth, however, several sizes become predominant with the result that stating an average island size for a definite quantity of metal loses meaning.

3. It is suggested that when an impinging vapor atom lands within a defined area surrounding each nucleus, there is a high probability that the atom will become incorporated into the nucleus before re-evaporating from the substrate or colliding with another nucleus. Following fresh nucleation, the extent of the

surrounding area is determined from the distance halfway between two small nuclei.

4. Substrates prepared in situ and immediately prior to metal deposition provide an atomically clean surface for film studies. The indium films deposited on such substrates show growth characteristics which differ little from the films obtained with air-exposed substrates. Generally, certain island sizes are predominant from one growth stage to the next, and as many as four overlapping stages contain similar sets of predominant sizes in the region of overlap.

5. Shoulders on the peaks of predominant island sizes indicate that growth of larger islands is favored over the smaller ones. For 1000Å islands, growth rates by surface atom diffusion are within an order of magnitude from one another. Growth by direct addition becomes increasingly more important as the island size increases beyond 1000Å.

6. The contact angles for indium, lead and lead plus indium as measured on the 'three-dimensional' electron micrographs are essentially the same. Since the geometry of the film islands is cap-shaped over a range of sizes from 100Å to 1000Å, it is assumed that the critical nucleus is also cap-shaped.

7. The deposition rate for indium films is very sensitive to the filament temperature and hence to the temperature of the evaporating metal.

VI. PROPOSED WORK

There are a number of important experiments which would extend and broaden the scope of this study and contribute to the understanding of the growth and structure of metal films. One of the most pressing needs in the study of thin metal films is an acceptable, unambiguous means of stating the thickness of films present on the substrate.

It is suggested, therefore, that primary effort be devoted to the establishment of a film quantity expression whose measurement is highly reproducible. The units of quantity chosen for this study are cycles per second, the frequency change of a quartz crystal thickness monitor. The major advantages of using a monitor are; (1) it is extremely simple to install and operate, (2) it provides continuous measurements during the film growth, (3) the results are reproducible, and (4) minute changes in the deposition rate are quickly detectable and can be corrected either manually or automatically.

Included among the disadvantages are the following; (1) the drift in frequency over a period of time can be as much as 10 cps per hour, (2) the monitor is sensitive to temperature changes, and (3) thickness measurements

obtained from the monitor generally refer to the quantity of film deposited upon a substrate which is the same material as the film.

The frequency drift is inherent in the design and construction of the instrument and may be improved by changes in the monitor's circuitry. Temperature variations may be reduced by cooling the sensing head with water; however, in that case, the mobility of the sensor is limited. The third disadvantage concerning the meaning of the monitor data may be overcome if the substrate material can be deposited on the monitor prior to film formation. From the change in slope of the deposition rate, a sticking coefficient for the substrate may be calculated. Therefore, corrections in the monitor reading can be used to determine the actual quantity of film material present during the initial nucleation period.

The investigation of bimetallic films is proposed as an experiment for determining intermetallic diffusion constants for metal films. The study of intermetallic diffusion employing thin films would provide insight into the structure of deposited films, as well as a rapid estimate of the bulk diffusion constant for bimetallic systems at very low temperatures. Other aspects of bimetallic systems worthy of consideration are the mechanisms involved in the interaction of one metal deposited on another.

The importance of island evaporation as a technique for studying the formation of metal films merits some consideration. A metal film prepared in an ultra high vacuum may be examined in an electron microscope without the contamination problems which generally plagued *in situ* film growth studies. The evidence of nuclei present under the evaporated islands suggests a second mode of growth through condensation on a seed crystal attached to the substrate. If such a mechanism is responsible for the presence of the islands which evaporated, then perhaps a new understanding of epitaxial film growth may result.

VII. LIST OF REFERENCES

1. R. W. Wood, Phil. Mag. 30, 300 (1915); 32, 364 (1916).
2. I. Langmuir, Proc. Nat'l. Acad. Sci., Washington 3, 141 (1917).
3. R. E. Thun, "Structure of Thin Films," Physics of Thin Films, Vol. I, ed. George Hass, N.Y., Academic Press (1963).
4. J. Edgecumbe, J. Vac. Sci. Tech. 3, 28 (1966).
5. D. W. Pashley, and M. J. Stowell, Fifth International Congress for Electron Microscopy (1962).
6. J. v. d. Waterbeemd, J. Phys. Letters 16 (2), 97 (1965).
7. T. A. McLauchlan, R. S. Sennett, and G. D. Scott, Canad. J. Res., 28, 530 (1950).
8. R. D. Gretz, and G. M. Pound, "Vapor Solid Nucleation", Ph.D. Thesis (1963).
9. J. L. Robins, and T. N. Rhodin, Tech. Rep't. No. 8, Contract No. Nonr-401 (31) (1964).
10. J. P. Hirth, and G. M. Pound, Condensation and Evaporation, Nucleation and Growth Kinetics, Pergamon Press (1963).
11. J. P. Hirth, and G. M. Pound, J. Chem. Phys. 26, 1216 (1957).
12. I. Langmuir, Phys. Rev. 2, 329 (1913).
13. B. Siegel, Quart. Revs. 19, 77 (1965).
14. J. P. Hirth, Ann. New York Acad. Sci. 101, 805 (1963).
15. J. W. Gibbs, Collected Works, Vol. I, "Thermodynamics", Yale University Press, New Haven (1948) p. 219.

16. M. Volmer, Kinetik der Phasenbildung, Steinkopff, Dresden and Leipzig (1939).

17. K. L. Moazed, and J. P. Hirth, Surf. Sci. 3, 49 (1964).

18. J. P. Hirth, Acta. Met. 7, 755 (1959).

19. R. Becker, and W. Doering, Ann. Physik 24, 719 (1935).

20. G. M. Pound, M. T. Simnad, and L. Yang, J. Chem. Physics 22, 1215 (1954).

21. J. P. Hirth, S. J. Hruska, and G. M. Pound, Proc. Conf. Single Crystal Films, Pennsylvania (May, 1963) p. 9.

22. T. N. Rhodin, and D. Walton, Metal Surfaces: Structures, Energetics and Kinetics, American Society for Metals, Metals Park, Ohio (1963) Ch. 8.

23. M. Volmer, and A. Weber, Phys. Chem. 119, 277 (1925).

24. L. Yang, C. E. Birchenall, G. M. Pound, and M. Simnad, Acta. Met. 2, 462 (1954).

25. D. Walton, J. Chem. Phys. 37, 2182 (1962); Phil. Mag. 7, 1671 (1962).

26. J. Lothe, and G. M. Pound, J. Chem. Phys. 36, 2080 (1962).

27. C. Sella, P. Conjeaud, and J. J. Trillat, Proc. Fourth International Conf. on Electron Microscopy, Vol. I, Berlin (1958) p. 508.

28. G. A. Bassett, Phil. Mag. 3, 72 (1958).

29. G. A. Bassett, J. W. Menter, and D. W. Pashley, Structure and Properties of Thin Films, C. A. Neugebauer, J. B. Newkirk and D. A. Vermilyea, eds., John Wiley & Sons, Inc., New York (1959) p. 11.

30. R. M. Hill, Nature 210 (5035), 512 (1966).

31. L. Bruck, Ann. Phys. 418, 233 (1936).

32. S. Shirai, Proc. Phys. Math. Soc. Japan 25, 168, 633 (1943).

33. J. H. van der Merwe, Proc. Conf. Single Crystal Films, Pennsylvania (May, 1963).

34. F. G. Allen, J. Eisinger, H. D. Hagstrum, and J. T. Law, J. Appl. Phys. 30, 1563 (1959).

35. R. W. Roberts, Brit. J. Appl. Phys. 14, 537 (1963).

36. L. Holland, Brit. J. Appl. Phys. 9, 410 (1958).

37. L. Holland, Vacuum Deposition of Thin Films, Chapman and Hall, Ltd., London (1963).

38. H. L. Caswell, J. Appl. Phys. 32, 2641 (1966).

39. C. Sella, and J. J. Trillat, Proc. Conf. Single Crystal Films, Pennsylvania (1963).

40. R. H. Jeppesen, and H. L. Caswell, IBM Journal (Oct., 1963) p. 297.

41. G. P. Motulevich, and A. A. Shubin, Soviet Physics JETP 17, (1) 33 (1963).

42. A. Fick, Pogg. Ann. 94, 59 (1855).

43. W. Jost, Diffusion in Solids, Liquids, Gases, Academic Press, Inc., New York (1952).

44. C. Weaver, and R. W. Hill, Adv. Phys. 8. 375 (1959).

45. P. M. Schaible, and L. I. Maissel, Trans. Ninth Nat'l. Vac. Symp. (1962) p. 190.

46. S. Dushman, Vacuum Technique, Wiley, New York (1949).

47. A. E. Barrington, High Vacuum Engineering, Prentice-Hall, Inc., Englewood Cliffs, New Jersey (1963).

48. G. Lewis, Fundamentals of Vacuum Science and Technology, McGraw-Hill Book Co., New York (1965).

49. H. L. Caswell, "Ultra High Vacuum Evaporators and Residual Gas Analysis," Physics of Thin Films, Vol. I, ed. G. Hass, Academic Press, New York (1963).

50. J. D. Blades, J. Gerber, and C. T. Thompson, ONR Symposium Rep't. A. C. R. - 50, (1960) p. 121.

51. W. R. Wheeler, and M. Carlson, 1961 Vac. Symp. Trans., 1309 (1962).

MICHIGAN STATE UNIVERSITY LIBRARIES
3 1293 03082 8614